

# Abnormal Driving Behavior Recognition Method Based on Smart Phone Sensor and CNN-LSTM

Hao Li

College of Electromechanical  
Engineering  
Qingdao University of Science  
and Technology  
Qingdao, China

Junyan Han

College of Electromechanical  
Engineering  
Qingdao University of Science  
and Technology  
Qingdao, China

Shangqing Li

College of Electromechanical  
Engineering  
Qingdao University of Science  
and Technology  
Qingdao, China

Hanqing Wang

College of Electromechanical  
Engineering  
Qingdao University of Science  
and Technology  
Qingdao, China

Hui Xiang

College of Electromechanical  
Engineering  
Qingdao University of Science  
and Technology  
Qingdao, China

Xiaoyuan Wang

College of Electromechanical  
Engineering  
Qingdao University of Science  
and Technology  
Qingdao, China

---

**Abstract:** Accurate identification of abnormal driving behavior is very important to improve driver safety. Aiming at the problem that threshold or traditional machine learning methods are mostly used in existing studies, it is difficult to accurately identify abnormal driving behavior of vehicles, a method of abnormal driving behavior recognition based on smartphone sensor data and convolutional neural network (CNN) combined with long and short-term memory (LSTM) was proposed. Smartphone sensors are used to collect vehicle driving data, and data sets of various driving behaviors are constructed by preprocessing the data. A recognition model based on a convolutional neural network combined with a long short-term memory network was constructed to extract depth features from data sets and recognize abnormal driving behaviors. The test results show that the accuracy of the model based on CNN-LSTM can reach 95.22%, and the performance indexes can reach more than 94%. Compared with the recognition model constructed only by CNN or LSTM, this model has higher recognition accuracy.

**Keywords:** Identification of abnormal driving behavior; Smartphone sensor; Convolutional Neural Network; Long Short-Term Memory

---

## 1. INTRODUCTION

With the rapid development of the automobile manufacturing industry and the improvement of people's living standards, the number of cars has continued to grow. The popularization of private cars has brought great convenience to people's daily travel and also caused a large number of traffic accidents. Expert analysis results show that driver's factors are the main factors that cause traffic accidents, and controlling driver's behaviors is an effective means to improve vehicle safety [1,2]. Therefore, accurate identification of abnormal driving behaviors can effectively improve driver safety and reduce the incidence of traffic accidents, which is of great significance to improving road traffic safety.

At present, there are three main methods of driving behavior recognition research by scholars at home and abroad: one is the method of driving behavior recognition based on visual images. Jain et al. used cameras to record drivers' facial features and corresponding road condition information during steering or lane change, and used a hidden Markov model to predict vehicle driving behavior [3]. Zhang et al. used vehicle-mounted cameras to collect video images and proposed an interwoven deep convolutional neural network architecture for real-time and accurate recognition of driver behavior [4].

Although the method of driving behavior recognition based on visual images may produce good results in some scenes. But in practical application, this method is easily affected by light and weather and has high environmental dependence. The second is the method of driving behavior recognition based on the vehicle-mounted or external equipment. Ding et al. proposed a driver's distracted driving behavior detection method based on a frequency modulated continuous wave radar system [5]. Yao et al. collected behavioral data of taxi drivers based on onboard diagnosis system and onboard positioning system, realized initial clustering through dynamic time warping algorithm and hierarchical clustering, and put the clustering results into hidden Markov model to identify driving behaviors [6]. Wang et al. proposed a driver fatigue behavior evaluation system based on EEG signals and integrated learning methods [7]. Recognition methods based on vehicles-mounted or external devices can achieve better recognition accuracy, but the installation and arrangement of these devices are cumbersome and require a certain cost, and some devices are intrusive to the driver. The third is the method of driving behavior recognition based on smartphones sensors. Johnson et al. integrated the sensor data of the accelerometer, gyroscope, and magnetometer in the smartphone based on the dynamic time warping algorithm for

the detection, recognition and recording of dangerous driving behaviors [8]. Xu et al. used the built-in audio sensor device of the mobile phone to realize the early recognition of the driver's distracted driving behavior [9]. Yu et al. used smartphone sensors to monitor abnormal driving behavior and adopted a support vector machine and neural network to realize fine-grained abnormal driving behavior monitoring and recognition [10]. Wu et al. collect bus acceleration, direction change and driving time data through smartphone acceleration and direction sensors, and detect and recognize abnormal bus driving behaviors based on the Naive Bayes algorithm [11]. Compared with the above two methods, the method of driving behavior recognition based on the smartphones sensor is more convenient and economical. Meanwhile, the network transmission technology and computing function of smartphones provide the possibility for further processing and in-depth analysis of the data collected in real-time. However, most of the existing research on this type of method is based on thresholds or traditional machine learning algorithms for driving behavior recognition, the recognition accuracy is not high and the generalization ability of the model is poor.

Given this, a recognition method of abnormal driving behavior based on smartphone sensors and convolutional neural network (CNN) combined with long short-term memory (LSTM) is proposed. The mobile phone sensor collects real-time vehicle driving data, the sliding window method is used to process the preprocessed time series data to generate "sample pictures". By constructing a convolutional neural network combined with a long short-term memory network model, deep feature extraction of driving behavior data and accurate recognition of abnormal driving behaviors are realized.

## 2. OVERALL IDENTIFICATION METHOD FRAMEWORK

The recognition method of vehicle abnormal driving behavior proposed in this paper mainly includes three parts: data collection, data processing, and abnormal driving behavior recognition. Firstly, the vehicle-mounted mobile phone sensor is used to collect the data of abnormal driving behavior. Then, the coordinate system of the mobile phone is adjusted and aligned with the coordinate system of the car body, and the obtained sensor parameters are corrected to the coordinate system parallel to the car body, and data filtering and normalization processing are carried out successively. Finally, the driving behavior data is divided into N "sample pictures" by the sliding window method, input into the convolutional neural network for deep feature extraction, and the extracted deep features are sent to the long short-term memory network for abnormal driving behavior recognition. The framework of the overall recognition method is shown in Figure 1.

## 3. EXPERIMENTAL DATA COLLECTION AND PROCESSING

### 3.1 Smart Phone Sensor Data Collection

To analyze the movement characteristics of the vehicle in different driving conditions, smartphone sensors are used to collect vehicle dynamic data, mainly including acceleration sensor data  $A_x, A_y, A_z$ , which represent the acceleration of the phone's X-axis, Y-axis, and Z-axis; gyroscope sensor data  $G_x, G_y, G_z$ , which represent the angular velocity around

the X-axis, Y-axis, and Z-axis of the mobile phone; the mobile phone attitude angle obtained by fusing the magnetic field sensor data and the acceleration sensor data: pitch, roll, yaw, Where pitch is the angle between the positive direction of the Y-axis and the horizontal direction when the phone rotates around the X-axis, the roll is the angle between the positive direction of the X-axis and the horizontal direction when the phone rotates around the Y-axis, and yaw is the angle when the phone rotates around the Z-axis, The angle between the positive direction of the Y-axis and the north direction of the magnetic field.

Before data collection, the mobile phone is first placed in the car with a bracket to make the mobile phone face up and the Y-axis is parallel to the front of the car. The coordinate system of the mobile phone is aligned with the coordinate system of the car body, which is called "standard posture" [12], as shown in Figure 2. Since the vehicle will produce different motion states during the driving process, it cannot be guaranteed that the vehicle-mounted mobile phone will be placed in strict accordance with the standard posture. Therefore, it is necessary to perform real-time rotation correction on the vehicle-mounted mobile phone sensor data and rotate it to the data in the "standard attitude" shown in Figure 2.

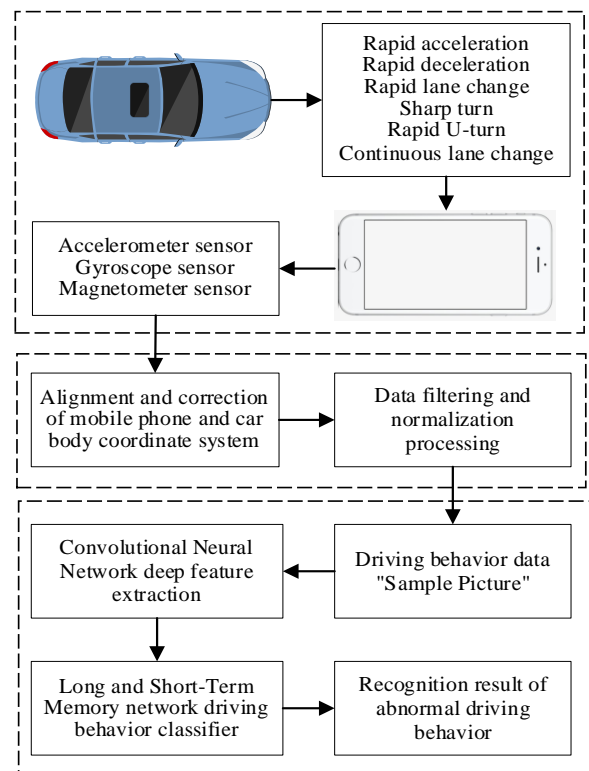


Figure 1 The framework of the overall recognition method

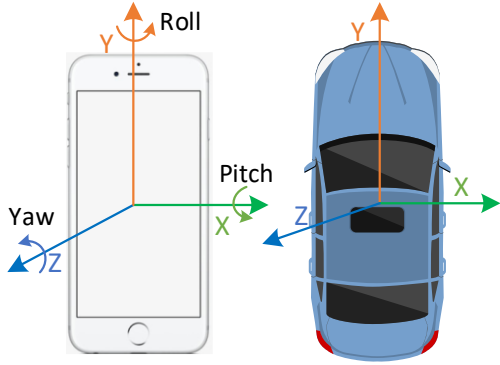


Figure 2 Coordinate alignment

The conversion of the three-axis acceleration and angular velocity in the non-standard posture into the corresponding data under the standard posture is regarded as a three-dimensional coordinate rotation problem, which is decomposed into the superposition of the three coordinate axis rotations, and then converted into a matrix transformation problem [12]. In this paper, the most commonly used method of coordinate axis rotation: "yaw-pitch-roll" method, the rotation formula to convert the non-standard posture coordinate system to the standard posture coordinate system can be obtained by formula (1). The sensor data collected under a non-standard attitude can be converted to the corresponding sensor data under standard attitude by using Formula (2).

$$R = R_z(\varphi)R_x(\alpha)R_y(\beta) = \quad (1)$$

$$\begin{bmatrix} \cos \varphi & \sin \varphi & 0 \\ -\sin \varphi & \cos \varphi & 0 \\ 0 & 0 & 1 \end{bmatrix} \begin{bmatrix} 1 & 0 & 0 \\ 0 & \cos \alpha & \sin \alpha \\ 0 & -\sin \alpha & \cos \alpha \end{bmatrix} \begin{bmatrix} \cos \beta & 0 & -\sin \beta \\ 0 & 1 & 0 \\ \sin \beta & 0 & \cos \beta \end{bmatrix} =$$

$$\begin{bmatrix} R_{11} & \sin \varphi \cos \alpha & R_{13} \\ R_{21} & \cos \varphi \cos \alpha & R_{23} \\ \cos \alpha \sin \beta & -\sin \alpha & \cos \alpha \cos \beta \end{bmatrix}$$

$$X' = RX \quad (2)$$

Where  $R_x(\alpha)$  is the X-axis rotation matrix,  $R_y(\beta)$  is the Y-axis rotation matrix, and  $R_z(\varphi)$  is the Z-axis rotation matrix,

$$R_{11} = \cos \varphi \cos \beta + \sin \varphi \sin \alpha \sin \beta,$$

$$R_{21} = -\sin \varphi \cos \beta + \cos \varphi \sin \alpha \sin \beta,$$

$$R_{13} = -\cos \varphi \sin \beta + \sin \varphi \sin \alpha \cos \beta,$$

$$R_{23} = \sin \varphi \sin \beta + \cos \varphi \cos \alpha \cos \beta.$$

When the mobile phone coordinate system is aligned with the vehicle coordinate system, and data rotation correction is performed, the movement state of the vehicle body can be characterized by the data of the built-in sensor of the smartphone. To analyze the dynamic parameter characteristics of the vehicle-mounted mobile phone under different abnormal driving behaviors of the vehicle, the sensors data of the mobile phone under the seven motion states of the

vehicle's rapid acceleration, rapid deceleration, rapid lane change, sharp turn, rapid U-turn, continuous lane change and normal driving are collected. The experimental data contains 8 characteristic variables, including three-axis acceleration data  $A_x, A_y, A_z$  and three-axis combined acceleration  $A_s$ ; three-axis angular velocity data  $G_x, G_y, G_z$ , and three-axis combined angular velocity  $G_s$ . The calculation formulas of three-axis combined acceleration  $A_s$  and three-axis combined angular velocity  $G_s$  are as follows.

$$A_s = \sqrt{A_x^2 + A_y^2 + A_z^2} \quad (3)$$

$$G_s = \sqrt{G_x^2 + G_y^2 + G_z^2} \quad (4)$$

During the experimental data collection process, the time when the specific abnormal driving behavior occurred and the corresponding tags were artificially recorded. Normal driving, rapid acceleration, rapid deceleration, rapid lane change, sharp turn, rapid U-turn, and continuous lane change are represented by 0-6 labels respectively.

### 3.2 Data Processing

In the process of experimental data collection, due to the complex road conditions, the vehicle's own vibration and sensor accuracy, a certain amount of high-frequency noise will appear in the collected raw sensor data. Therefore, before analyzing the variation characteristics of various abnormal driving behaviors in acceleration and direction angle, the collected original data should be filtered to eliminate high-frequency noise. In this paper, a sliding mean filter algorithm is used to smooth and filter the sensor data, and the mean filter expression is shown in the formula:

$$\bar{X}_n = \frac{1}{M} \sum_{i=0}^{M-1} X_{n-i} \quad (5)$$

Where  $M$  is the sliding filter window size, and  $X_{n-i}$  is the  $n-i$  th original data. The filter window  $M$  will have a greater impact on the filtering effect. According to the original data collection frequency (50Hz), we choose  $M = 10$  to smooth the original data.

Through the analysis of the filtered sensor data, it is found that the dimension of each sensor feature data is different, which easily affects the target result. Therefore, the original sensor feature data is normalized to map the result value of the feature data to  $[0,1]$ . The function is shown in Equation 6.

$$a' = \frac{a - \min a}{\max a - \min a} \quad (6)$$

Where  $a$  is the original data, and  $a'$  represents the normalized value of the input sample  $a$ .

## 4. MODEL

### 4.1 Convolutional Neural Network (CNN)

CNN is one of the most important networks in the field of deep learning. CNN is a feedforward neural network that can extract features from data with a convolutional structure [13]. Its basic structure consists of an input layer, a convolutional layer, a pooling layer, a fully connected layer, and an output layer [14]. The convolutional layer performs deep feature

extraction on the original data through local connections, meanwhile reducing the original data dimension. The pooling layer is also called the down-sampling layer, which can effectively reduce the complexity of the network, reduce the number of training parameters, and play the role of secondary feature extraction and dimensionality reduction. The fully connected layer can integrate the local information with classification in the convolutional layer or the pooling layer. The basic network structure of CNN is shown in Figure 3.

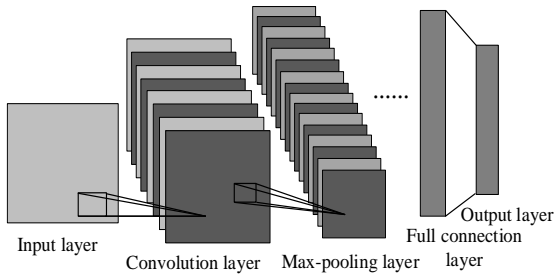


Figure 3 Basic network structure of the convolutional neural network

#### 4.2 Long Short-Term Memory (LSTM)

In order to solve the long-term dependency problem of Recurrent Neural Network (RNN) [15], Hochreiter et al. proposed an improved RNN in 1997 [16], that is, long short-term memory (LSTM), which uses a unique gate structure to effectively solve the problem of gradient explosion and gradient disappearance in RNN. LSTM has shown excellent performance in the recognition and prediction of time series data. Therefore, in this study, LSTM was selected to analyze the driving behavior characteristic data with time series.

Each layer of the LSTM network is composed of cyclically linked unit blocks, which mainly include three gate structures: forget gates, input gates, and output gates [17]. The network unit block structure of this study is shown in Figure 4. The forgetting gate determines how much information about the memory cell state  $C_{t-1}$  at the previous moment is retained; the input gate updates the characteristic information according to  $h_{t-1}$  and  $X_t$ , and combines it with the memory cell state  $C_{t-1}$  at the previous moment. It is the new memory cell state  $C_t$ ; the output gate determines how much current information can be output.

The calculation formula of the LSTM neuron is as follows:

$$f_t = \sigma(W_f \cdot [h_{t-1}, X_t] + b_f) \quad (7)$$

$$i_t = \sigma(W_i \cdot [h_{t-1}, X_t] + b_i) \quad (8)$$

$$\hat{C}_t = \tanh(W_c \cdot [h_{t-1}, X_t] + b_c) \quad (9)$$

$$C_t = f_t * C_{t-1} + i_t * \hat{C}_t \quad (10)$$

$$o_t = \sigma(W_o \cdot [h_{t-1}, X_t] + b_o) \quad (11)$$

$$h_t = o_t * \tanh(C_t) \quad (12)$$

Where  $f_t$ ,  $i_t$ ,  $o_t$  are forget gate, input gate, and output gate respectively,  $X_t$ ,  $\hat{C}_t$ ,  $h_{t-1}$ ,  $h_t$  are input value, candidate state value, previous hidden layer output, this hidden layer output

respectively,  $W_f$ ,  $W_i$ ,  $W_c$ ,  $W_o$  are the weights of the corresponding gates respectively,  $b_f$ ,  $b_i$ ,  $b_c$ ,  $b_o$  are the biases of the corresponding gates respectively,  $\sigma$  represents the sigmoid activation function, and  $\tanh$  represents the nonlinear activation function.

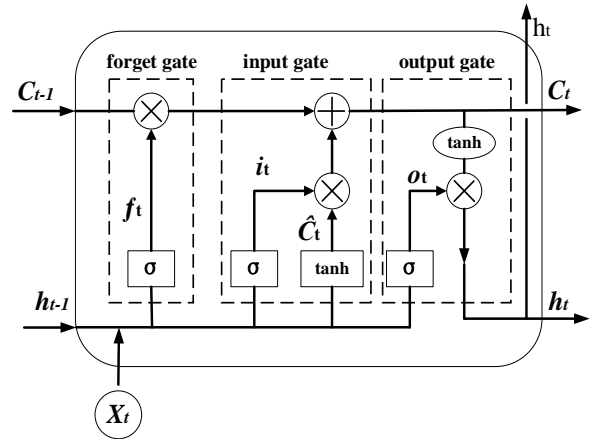
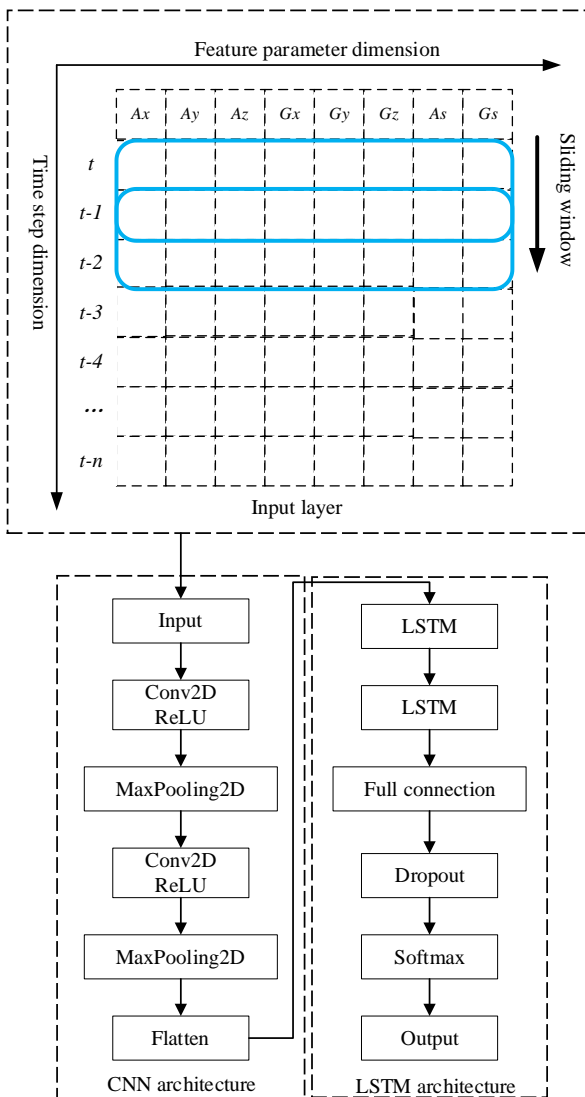


Figure 4 Unit structure of LSTM network

#### 4.3 Recognition Model of Vehicle Abnormal Driving Behavior Based on CNN-LSTM

Taking into account the advantages of convolutional neural networks and long short-term memory networks in feature extraction and processing dynamic timing information, this paper constructs a recognition model of vehicle abnormal driving behavior based on CNN and LSTM. The basic framework is shown in Figure 5. First, use the sliding window method to divide the smartphone sensor data into time series, construct a two-dimensional driving behavior feature data "sample picture" and transmit it to the input layer of the convolutional neural network; through the convolutional layer, the deeper features in the original data are processed. Extract and use the pooling layer to perform feature dimensionality reduction, reduce the complexity of the network, and finally obtain the optimal driving behavior feature parameters. Then, LSTM was used to construct the model and analyze the depth characteristic parameters extracted by CNN on time series. Finally, Softmax classifier is used to classify and identify driving behaviors, which are divided into seven categories: rapid acceleration, rapid deceleration, rapid lane change, sharp turn, rapid U-turn, continuous lane change and normal driving.



**Figure 5 Basic framework of abnormal driving behavior recognition model based on CNN-LSTM**

(1) Input layer. The pre-processed driving behavior data: X-axis acceleration  $A_x$ , Y-axis acceleration  $A_y$ , Z-axis acceleration  $A_z$ , X-axis angular velocity  $G_x$ , Y-axis angular velocity  $G_y$ , Z-axis angular velocity  $G_z$ , triaxial acceleration  $A_s$  and triaxial angular velocity  $G_s$  were connected in series into the time series feature vectors of 8 dimensions. According to the time series, the data per second is expressed as a two-dimensional matrix of "time step  $\times$  feature vector", and the "sample picture" of driving behavior data is generated on the data set by sliding window in accordance with the data division method of input layer in the above figure. The sensor data (acquisition frequency is 50Hz) is traversed with a 2-second sliding window and a 1-second sliding step, and N sample pictures of "100 $\times$ 8" pixels are generated. Where 100 is 100 sensor data collected within 2 seconds, 8 is the dimension of the input feature vector, and the number of sample pieces is N.

(2) CNN architecture. The processed "sample pictures" of the input layer are sent to the convolutional neural network, and CNN is used for feature extraction. The CNN architecture consists of an input layer, two convolutional layers, two pooling layers and a flatten layer. In the two convolutional layers, the number of convolution kernels is 16, 32, and the size is 3 $\times$ 3. The step size is 1 in both the time step dimension and the feature parameter dimension. A filling is used, and the ReLU activation function is selected for activation. In the two pooling layers, the pooling core size is 2 $\times$ 2, the step size is 2 in both the time step dimension and the feature parameter dimension, and the maximum pooling principle is selected. In order to alleviate the over-fitting phenomenon and speed up the training speed of the neural network, a Batch Normalization layer is added after each layer of the convolutional layer. Finally, through the Flatten operation, the deep abstract features extracted are converted into global feature vectors as the input of the LSTM layer.

(3) LSTM architecture. LSTM is used to train the global feature variables extracted by CNN. After adjustment and testing, it can be known that the 2-layer LSTM structure achieves the best prediction effect. The number of LSTM neurons is 64 and 128 respectively. The number of neurons in the fully connected layer is also set to 128. The dropout layer has a loss rate of 0.5. The role of this layer is to alleviate the over-fitting phenomenon of the model. Finally, the probability of each driving behavior category is output through the Softmax activation function of the output layer.

## 5. EXPERIMENT AND ANALYSIS

### 5.1 Model Training

In this study, a neural network model was built based on Keras deep learning framework and Python3.7 programming language. The experimental platform configuration is: Intel(R)Core(TM) i7-10870H CPU @ 2.20GHz, memory for 16G, graphics card for GTX3060 Laptop, video memory for 6G.

The total number of original data samples selected in the experiment is 121,000. After the combined screening, 2400 "sample pictures" are generated, which including 1200 normal driving data, rapid acceleration data, rapid deceleration data, rapid lane change data, sharp turn data, rapid U-turn data and continuous lane change data are 200 sheets each. The data set is divided into training set and test set according to the ratio of 7:3. The identification of abnormal driving behavior in this study is a multi-classification problem, so the label needs to be One\_hot encoded first.

After the initial network model is constructed, the network parameters need to be set and adjusted before the model is trained. In this paper, the Adam optimization algorithm is selected to adjust and optimize the model parameters. At the same time, in order to prevent the model from falling into a local minimum, the learning rate is set to 0.001, and the number of iterations of the model epochs is set to 1000. The model's accuracy rate change and loss function value convergence during the training process are shown in Figures 6 and 7. It can be seen from Figure 6 that the recognition accuracy of the CNN-LSTM model can reach more than 95%, achieving high recognition accuracy. The change of the loss function can also reflect the training effect of the algorithm model. It can be seen from Figure 7 that as the number of training increases, the loss function of the CNN-LSTM model

converges faster. After 300epoch, the convergence tends to be flat, and the loss value is close to 0.04, with better identification performance.

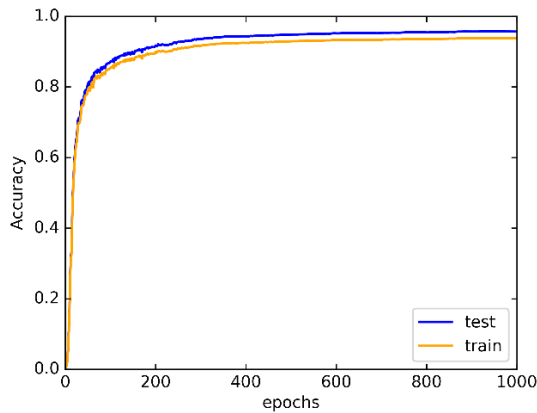
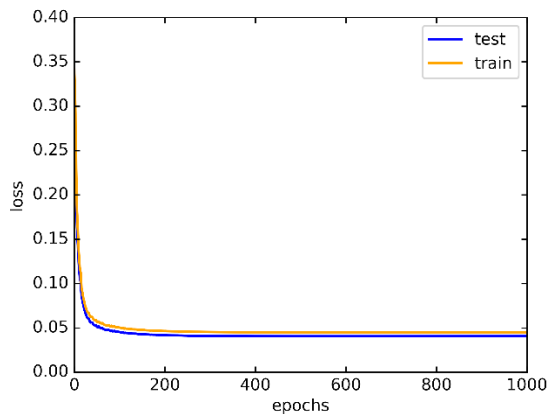


**Figure 6 The recognition accuracy of the CNN-LSTM model**



**Figures 7 Loss change curve of CNN-LSTM model**

## 5.2 Model Testing and Comparison

In order to evaluate the overall performance of the CNN-LSTM model for the recognition of abnormal driving behaviors, all types of abnormal driving behaviors are regarded as one type, and only one type of driving behavior is identified whether it is abnormal or normal. We define the evaluation indicators of the following models according to True Positive (TP), True Negative (TN), False Positive (FP), and False Negative (FN) [18]:

Accuracy: reflects the accuracy of the model's recognition of various driving behaviors, that is, the ratio of the number of samples correctly classified by the classifier to the total number of samples.

$$Accuracy = \frac{TP + TN}{TP + TN + FP + FN} \quad (13)$$

Precision: reflects the proportion of real A-type driving behavior in the sample predicted by the model to be A-type driving behavior.

$$Precision = \frac{TP}{TP + FP} \quad (14)$$

Recall: reflects the model's proportion of all Class A driving behavior samples recognized as Class A.

$$Recall = \frac{TP}{TP + FN} \quad (15)$$

F1-Score: A comprehensive indicator of the balance between accuracy and recall, which is a weighted average of model accuracy and recall.

$$F-1 = \frac{2 \cdot precision \cdot recall}{precision + recall} \quad (16)$$

The identification results of the model were calculated and analyzed according to the above formula. The overall identification accuracy of the model was 95.22%, and the details of other evaluation indicators of the model were shown in Table 1. The model has a better recognition effect on all abnormal driving behaviors, and the Recall can reach 95.83%. All the performance indexes of normal driving behaviors and abnormal driving behaviors identified by the model are more than 94%, and the F1-Score performance indicators exceeded 95%. The model achieved good recognition results.

**Table 1 Various evaluation indicators of CNN-LSTM model**

Evaluation index	Precision (%)	Recall (%)	F1-Score (%)
Normal driving behavior	95.79	94.72	95.25
Abnormal driving behavior	94.78	95.83	95.31

In order to further evaluate the accuracy of the model's recognition of the six abnormal driving behaviors, 80 sets of data for each of rapid acceleration (RA), rapid deceleration (RD), sharp turning (ST), rapid lane change (RLC), rapid U-turn (RU), and continuous lane change (CLC) driving behavior were selected to construct a new test set and input them respectively the trained CNN-LSTM model is recognized. The recognition results are shown in Table 2.

**Table 2 Recognition accuracy rate of six abnormal driving behaviors**

driving behavior	RA	RD	ST
Accuracy (%)	96.25	97.5	93.75
driving behavior	RLC	RU	CLC
Accuracy (%)	95	92.5	93.75

It can be seen from Table 2 that the accuracy of the model for the recognition of six abnormal driving behaviors exceeds 92%, and a good recognition effect is achieved. Among them, the recognition accuracy of rapid acceleration and rapid deceleration driving behavior can reach more than 96%, and the recognition effect is the best. Because the data change lasts for a short time, the driving behavior can be completed within the sliding partition window time, so the recognition accuracy is high. Second, the changes time of driving behavior data of rapid U-turns, sharp turns, and continuous lane changes have a relatively long duration. The driving behavior may not be completed within the sliding partition

window, which will reduce the accuracy of the model's recognition.

In order to highlight the effectiveness and superiority of the CNN-LSTM abnormal driving behavior recognition model proposed in this paper, CNN and LSTM are used to process the same data samples respectively, and the abnormal driving behavior recognition model is established for comparison. In order to reduce the chance of experimental results, the same data set was used to train each network model for three times respectively, and the recognition results of the model, such as overall recognition Accuracy, recognition Precision of abnormal driving behavior, Recall of abnormal driving behavior and F1-Score, a comprehensive index of abnormal driving behavior, were averaged. The evaluation indicators of each model are shown in Table 3.

**Table 3 Evaluation index of each model**

Evaluation index	Accuracy (%)	Precision (%)	Recall (%)	F1-Score (%)
CNN	91.21	90.38	92.22	91.29
LSTM	92.82	92.01	93.79	92.89
CNN-LSTM	95.65	95.14	96.21	95.67

It can be seen from Table 3 that the recognition accuracy and comprehensive performance indicators of the LSTM model can reach about 93%. Compared with the CNN model, various performance indicators perform better. The CNN-LSTM model integrates the advantages of CNN depth feature extraction and LSTM for dynamic time-series information processing. Compared with the LSTM model, the recognition accuracy is increased by about 3%, and various performance indicators for abnormal driving behavior recognition are improved.

## 6. CONCLUSION

Accurate identification of abnormal driving behavior is of great significance to improve road traffic safety. Aiming at the problems of the poor accuracy of the abnormal driving behavior recognition method and the poor generalization ability of the model in the existing research. This paper proposes an abnormal driving behavior recognition method based on smartphone sensors and CNN-LSTM. The vehicle-mounted smartphone sensor data is used to characterize the movement characteristics of each driving behavior of the vehicle, and the acceleration and angular velocity sensor data are collected, and the driving behavior characteristic data set is constructed through the sensor data coordinate correction, data filtering, and data normalization processing. Given the advantages of CNN and LSTM networks in feature extraction and processing of dynamic timing information, a recognition model of vehicle abnormal driving behavior based on CNN and LSTM is constructed, and the effectiveness and accuracy of the model are verified by using feature data sets. Compared with the CNN and LSTM models, the results show that the performance indicators of the model have been improved and have higher recognition accuracy.

## 7. ACKNOWLEDGMENTS

This study was funded by the Qingdao Top Talent Program of Entrepreneurship and Innovation (Grant No.19-3-2-11-zhc), the Natural Science Foundation of Shandong Province (Grant No. ZR2020MF082), the Foundation of Shandong Intelligent Green Manufacturing Technology and Equipment Collaborative Innovation Center (Grant No. IGSD-2020-012), and the National Key Research and Development Project (Grant No.2018YFB1601500).

## 8. REFERENCES

- [1] Chan, T. K., Chin, C. S., Chen, H., & Zhong, X. (2019). A comprehensive review of driver behavior analysis utilizing smartphones. *IEEE Transactions on Intelligent Transportation Systems*, 21(10), 4444-4475.
- [2] Ellison, A. B., Greaves, S. P., & Bliemer, M. C. (2015). Driver behaviour profiles for road safety analysis. *Accident Analysis & Prevention*, 76, 118-132.
- [3] Jain, A., Koppula, H. S., Raghavan, B., Soh, S., & Saxena, A. (2015). Car that knows before you do: Anticipating maneuvers via learning temporal driving models. In *Proceedings of the IEEE International Conference on Computer Vision* (pp. 3182-3190).
- [4] Zhang, C., Li, R., Kim, W., Yoon, D., & Patras, P. (2020). Driver behavior recognition via interwoven deep convolutional neural nets with multi-stream inputs. *IEEE Access*, 8, 191138-191151.
- [5] Ding, C., Chae, R., Wang, J., Zhang, L., Hong, H., Zhu, X., & Li, C. (2019). Inattentive driving behavior detection based on portable FMCW radar. *IEEE Transactions on Microwave Theory and Techniques*, 67(10), 4031-4041.
- [6] Yao, Y., Zhao, X., Wu, Y., Zhang, Y., & Rong, J. (2021). Clustering driver behavior using dynamic time warping and hidden Markov model. *Journal of Intelligent Transportation Systems*, 25(3), 249-262.
- [7] Wang, P., Min, J., & Hu, J. (2018). Ensemble classifier for driver's fatigue detection based on a single EEG channel. *IET Intelligent Transport Systems*, 12(10), 1322-1328.
- [8] Johnson, D. A., & Trivedi, M. M. (2011, October). Driving style recognition using a smartphone as a sensor platform. In *2011 14th International IEEE Conference on Intelligent Transportation Systems (ITSC)* (pp. 1609-1615). IEEE.
- [9] Xu, X., Yu, J., Chen, Y., Zhu, Y., Qian, S., & Li, M. (2017). Leveraging audio signals for early recognition of inattentive driving with smartphones. *IEEE Transactions on Mobile Computing*, 17(7), 1553-1567.
- [10] Yu, J., Chen, Z., Zhu, Y., Chen, Y., Kong, L., & Li, M. (2016). Fine-grained abnormal driving behaviors detection and identification with smartphones. *IEEE transactions on mobile computing*, 16(8), 2198-2212.
- [11] Wu, X., Zhou, J., An, J., & Yang, Y. (2018, March). Abnormal driving behavior detection for bus based on the Bayesian classifier. In *2018 Tenth International Conference on Advanced Computational Intelligence (ICACI)* (pp. 266-272). IEEE.

- [12] Wang, R., Xie, F., Zhao, J., Zhang, B., Sun, R., & Yang, J. (2020). Smartphone Sensors-Based Abnormal Driving Behaviors Detection: Serial-Feature Network. *IEEE Sensors Journal*.
- [13] Li, Z., Liu, F., Yang, W., Peng, S., & Zhou, J. (2021). A survey of convolutional neural networks: analysis, applications, and prospects. *IEEE Transactions on Neural Networks and Learning Systems*.
- [14] LeCun, Y., Bottou, L., Bengio, Y., & Haffner, P. (1998). Gradient-based learning applied to document recognition. *Proceedings of the IEEE*, 86(11), 2278-2324.
- [15] Bengio, Y., Simard, P., & Frasconi, P. (1994). Learning long-term dependencies with gradient descent is difficult. *IEEE transactions on neural networks*, 5(2), 157-166.
- [16] Hochreiter, S., & Schmidhuber, J. (1997). Long short-term memory. *Neural computation*, 9(8), 1735-1780.
- [17] Jia, S., Hui, F., Li, S., Zhao, X., & Khattak, A. J. (2020). Long short-term memory and convolutional neural network for abnormal driving behaviour recognition. *IET Intelligent Transport Systems*, 14(5), 306-312.
- [18] Khodairy, M. A., & Abosamra, G. (2021). Driving Behavior Classification Based on Oversampled Signals of Smartphone Embedded Sensors Using an Optimized Stacked-LSTM Neural Networks. *IEEE Access*, 9, 4957-4972.

# A Statistical Model for Analyzing Anthropometric Data and Developing Clothing Sizing Systems for Libyan School Children

Salima A. Bilhassan  
 Benghazi University  
 Benghazi, Libya

Raja Albalaze  
 Benghazi University  
 Benghazi, Libya

Mariam Elgheriane  
 Benghazi University  
 Benghazi, Libya

Najat Elkwafi  
 Benghazi University  
 Benghazi Libya

**Abstract:** A garment sizing system is essential for effective clothing design and production. A sizing system classifies a specific population into homogeneous subgroups based on some key dimensions. Persons of the same subgroup have the same body shape characteristics, and share the same garment size. Anthropometric data plays important role in creating clothing sizing system. The current work represents the sixth step towards the overall goal of developing the Libyan children's clothing standards system based on physical measurements of the human body of Libyan schoolchildren. The objective of the current work is to study the physical measurements of students aged 6 to 17 years in the stages of primary, secondary. The body measurements of school children in Benghazi were collected and analyzed using simple statistics methods to understand the body ranges and current of student in all stages to develop the system sizing. The measurements were collected from previous projects. Some measurements were collected to complement a work of 90 (male and female) students between 6, 7 and 8 years old from a school in Benghazi. ANOVA test was used to determine differences between age groups.

**Keywords:** Anthropometric data; sizing system; children clothing; schoolchildren; Children anthropometry

## 1. INTRODUCTION

Anthropometry is the branch of the human sciences that deals with body measurement, such as size, shape, reach, strength and working capacity (Gupta, 2014; Qutubuddin et al, 2012). This science helps designers to create spaces and products that are more suitable for the users, by taking into consideration different body dimensions and different activity requirements (Viviani et al, 2018; Shiru and Abubakar, 2012; Dawal et al, 2012). There have been several attempts to describe and represent the characteristics of entire populations (Veitch et al, 2007; Viviani et al, 2018; Shiru and Abubakar, 2012; Dawal et al, 2012; Gupta, 2014; Qutubuddin et al, 2012). There are different factors, which affected sizing system, such as gender and age. Many researchers find that there are significant differences between gender and age among almost body measurements (Ariadurai et al., 2009; Bari et al., 2015; Beazley, 1999; Chung et al., 2007; Gupta and Gangadhar, 2004; Gupta and Zakaria, 2014; Kang et al., 2001; Lee, 2013; Muslim et al., 2014; Zakaria, 2011, Bilhassan et al, 2018 (a); Bilhassan, 2018 (b); Bilhassan et al, 2020).

This study is motivated by the need to examine anthropometric measurements among school children in Libya; it is customary in Libya to use Size charts developed from different countries. This article reports the sixth step towards the overall objective. The overall objective is to develop a size chart based on anthropometric body measurements of Libyan schoolchildren. This article covers the results of all grades (aged 6 to 17 years) in the basic education stage.

## 2. METHODOLOGY

This section explains the material and method used in this research.

### 2.1 Participants

The data was collected by students from previous projects, were used (6-17 years) (Alarody et al, 2016; Albarki, 2017; Elmabrouk, 2017; Boushagour, 2018; Elurfi et al, 2018). These data are 19 measurements and 30 students per age group. There was a lack of data for age group (6-7-8). Sample size includes a total of the 90 Libyan primary students (45 males and 45 females). The fifteen students are from each a grade. The students aged between 6 to 8 years. The sample was randomly selected from one public school in the city of Benghazi during the school year (2018/2019). Measurements were taken after getting permission from the officials and principals in each school and all students voluntarily participated in the study. Table 1 includes summary of number of students included in the study.

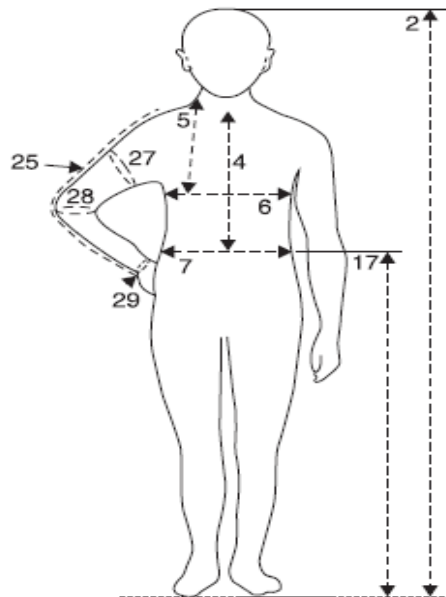
**Table 1. Summary of number of students included in the study**

School Name	Neighborhood	Total number measured						Total
		Grade						
		6		7		8		
		M	F	M	F	M	F	
ALNAJAH SCHOOL	AL FWAYHAT	15	15	15	15	15	15	90

<b>Total</b>	15	15	15	15	15	15	90
--------------	----	----	----	----	----	----	----

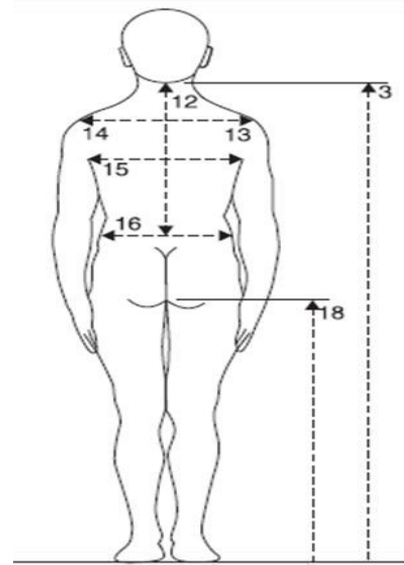
## 2.2 Body Measurements

Based on the objective of this project, only nineteen anthropometric dimensions are selected and used to establish the clothing sizing systems for students. These dimensions are selected based on previous studies (Ariadurai et al, 2009; Adu-Boakye et al, 2012; Alarody et al, 2016; Albarki et al, 2017; Elmabrouk et al, 2017; Boushagour et al, 2018; Elurfi et al, 2018; Bilhassan et al, 2018 (a); Bilhassan et al, 2018 (b); Bilhassan et al, 2019). Table 2 and Fig.1 to Fig.3 show the body dimensions. These measurements are used to make different types of clothing such as school uniforms. Readings were also taken two times and the average of the readings was recorded as the actual anthropometric measurements of the respondents.



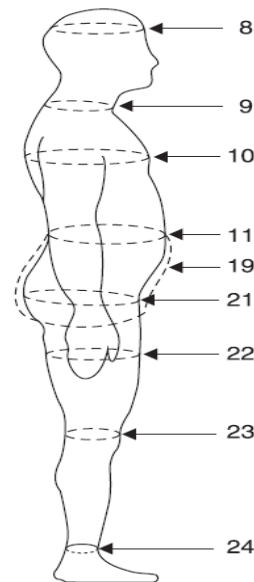
Code	Attribute
2	Height (Ht)
4	Centre front waist length (CFWL)
5	Highest shoulder to chest (HSC)
6	Front chest width (FCW)
7	Front waist (FW)
17	Waist height (WHt)
25	Arm length (ArL)
27	Upper arm girth (UARg)
28	Elbow girth (EG)
29	Wrist girth (WG)

Figure 1. Measures recorded from the front of the body (Gupta and Zakaria, 2014).



Code	Attribute
3	Cervical height (CerHt)
12	Centre back waist length (CBWL)
13	Arm hole depth (Ar.H.D)
14	Across back shoulder width (ABSW)
15	Across back width (ABW)
16	Back waist (BW)
18	Crotch height (CrHt)

Figure 2. Measures recorded from the back of the body (Gupta and Zakaria, 2014).



Code	Attribute
8	Head circumference (HC)
9	Mid-neck girth (MNG)
10	Chest girth (CG)
11	Waist girth (WG)
19	Crotch length (CrL)
21	Hip girth (HG)
22	Thigh girth (TG)
23	Knee girth (KG)
24	Ankle girth (AG)

Figure 3. Body girths or circumferences (Gupta and Zakaria, 2014).

**Table 2. The Anthropometric Dimension**

No.	Body Dimension
1	Weight
2	Height
3	Head circumference
4	Neck circumference
5	Waist circumference
6	Chest circumference
7	Hip circumference
8	Arm circumference
9	Shoulder to shoulder length
10	Shoulder to wrist length
11	Shoulder to waist length
12	Front body length
13	Back body length
14	Waist to hips length
15	Shoulder length
16	Front body width
17	Back body width
18	Calf circumference
19	Knee circumference

### 2.3 Anthropometric Data Analysis

The collected data was analyzed using Minitab 17.1 statistical software. Descriptive statistics (using Microsoft Excel) such as mean, median, mode, min., max. and standard deviation were calculated for each dimension. As expected, data for all measurements followed a normal distribution. The ANOVA test was conducted to identify differences between the age groups. The results from this test were used to develop the clothing sizing system (Adu-Boakye et al., 2012).

## 3. RESULTS AND DISCUSSION

### 3.1 Descriptive Analysis

As expected that all measurements follow a normal distribution. This study found that the mean height for male is (116.54, 123.99, 125.49, 137.40, 143.33, 147.15, 150.16, 154.32, 166.72, 169.08, 176.43, 176.43) cm for grade 6 to 17 respectively, while mean height for female respondents is (117.19, 126.17, 124.54, 139.70, 143.00, 152.63, 147.54, 158.59, 157.32, 158.70, 159.66, 159.33) cm for grade 6 to 17 respectively. The standard deviation (SD) for almost all dimensions is quite large, showing great variation in the measurements.

### 3.2 Differences of Anthropometric Measurements by Gender (T-test)

T-tests were carried out to identify differences between males and females of 6 to 17 years of age. T-tests were carried out to identify how many sizes are to be developed based on the results of the analysis (Gupta and Gangadhar, 2004). The following sections are presented the results of t-test.

#### 3.2.1 Differences of anthropometric measurements by gender (for all ages)

The results of t-test show that almost all of the anthropometric measurements have no significant differences between the genders of respondents for all age groups 6 to 17 years. These differences would not be considered in design the clothing

sizing systems that are appropriate for children of different gender. These results diverse comare with results found in other researchers (Bilhassan et al, 2018 (b); Bilhassan et al, 2019)

There are differences in the anthropometric measurements: waist circumference, Arm circumference, and Knee circumference. These differences would be considered to design clothing sizing systems for different gender (as shown in Table 3).

**Table 3. Differences of anthropometric measurements by gender**

MEASUREMET	P-Value	Sig.
1	0.86	Not sig
2	0.14	Not sig
3	0.35	Not sig
4	0.29	Not sig
5	0.012	Sig
6	0.004	Not sig
7	0.35	Not sig
8	0.007	Sig
9	0.63	Not sig
10	0.80	Not sig
11	0.40	Not sig
12	0.90	Not sig
13	0.139	Not sig
14	0.95	Not sig
15	0.09	Not sig
16	0.26	Not sig
17	0.58	Not sig
18	0.44	Not sig
19	0.028	Sig

#### 3.2.2 Differences of anthropometric measurements by gender (for ages group 6-11)

The results show that almost of the anthropometric measurements there are no differences significantly between the genders. These differences would not be considered to produce clothing that is appropriate for children of different genders. These results contrast with other researches (Bilhassan, 2018(b); Bilhassan (2019))

There are differences in the anthropometric measurements: neck circumference, waist circumference, and back body length as shown in Table 4.

#### 3.2.3 Differences of anthropometric measurements by gender (for ages groups 12-17)

The results of t-test show that almost all of the anthropometric measurements have significant differences between the genders of respondents for age groups 12 to 17 years. These differences would be considered in design.

There are no differences in the anthropometric measurements: chest circumference, hip circumference, arm circumference, shoulder to wrist length, and shoulder to waist length, front body length, waist to hips length, back body width, calf circumference and knee circumference. These differences would not be considered to design clothing sizing systems for different gender (as shown in Table 5).

### 3.3 Differences of Anthropometric Measurements by Age (ANOVA)

#### 3.3.1 Difference between anthropometric measurements for female for all ages groups

Table 6 shows that all of the anthropometric measurements have difference significantly between the ages of respondents. These differences would be considered to produce clothing that is appropriate for children of different ages. There are no differences in the anthropometric for all measurements.

**Table 4. Differences of anthropometric measurements by gender for age groups 6-11**

MEASUREMET	P-Value	Sig.
1	0.50	not sig
2	0.27	not sig
3	0.50	not sig
4	0	Sig
5	0	Sig
6	0.77	not sig
7	0.27	not sig
8	0.21	not sig
9	0.44	not sig
10	0.10	not sig
11	0.93	not sig
12	0.08	not sig
13	0	Sig
14	0.09	not sig
15	0.11	not sig
16	0.10	not sig
17	0.17	not sig
18	0.15	not sig
19	0.14	not sig

**Table 5. Differences of anthropometric measurements by gender for age groups 12-17**

MEASUREMET	P-Value	Sig.
1	0.64	not sig
2	0.05	not sig
3	0.24	not sig
4	0.83	not sig
5	0.52	not sig
6	0	Sig
7	0	Sig
8	0	Sig
9	0.60	not sig
10	0	Sig

11	0.03	Sig
12	0	Sig
13	0	Sig
14	0	Sig
15	0.41	not sig
16	0.12	not sig
17	0	Sig
18	0	Sig
19	0	Sig

#### 3.3.2 Difference between anthropometric measurements for female for ages groups 6-11 (ANOVA)

Table 7 shows that all of the anthropometric measurements have significant difference significant between the ages of respondents. These differences would be considered to produce clothing that is appropriate for children of different ages.

There are differences in the anthropometric measurements: weight, height, head circumference, neck circumference, waist circumference, chest circumference, shoulder to shoulder length, shoulder to wrist length, shoulder to waist length, front body length, back body length, waist to hip length, shoulder length, and front body width. These differences would be considered to design clothing sizing systems for different gender.

**Table 6. Differences of anthropometric measurements by age groups for female (ANOVA)**

MEASUREMET	P-Value	Sig.
1	0	Sig
2	0	Sig
3	0	Sig
4	0	Sig
5	0	Sig
6	0	Sig
7	0	Sig
8	0	Sig
9	0	Sig
10	0	Sig
11	0	Sig
12	0	Sig
13	0	Sig
14	0	Sig
15	0	Sig
16	0	Sig
17	0.03	Sig
18	0.02	Sig
19	0.01	Sig

**Table 7. Differences of anthropometric measurements by age groups 6-11 for female (ANOVA)**

MEASUREMET	P-Value	Sig.
1	<0.01	Sig
2	<0.01	Sig

3	<0.01	Sig
4	<0.01	Sig
5	<0.01	Sig
6	<0.01	Sig
7	0.51	not Sig
8	0.08	not sig
9	0.04	Sig
10	<0.01	Sig
11	<0.01	Sig
12	<0.01	Sig
13	0.03	Sig
14	0.03	Sig
15	0.04	Sig
16	0.13	Sig
17	0.06	not sig
18	0.05	not sig
19	0.05	not sig

### 3.3.3 Difference between anthropometric measurements for female for ages groups 12-17

The results of ANOVA show that almost all of the anthropometric measurements have significant differences between the genders of respondents for age groups 12 to 17 years. These differences would be considered in design. There are differences in the anthropometric for all measurements except back body width as shown in Table 8.

**Table 8. Differences of anthropometric measurements by age groups 12-17 for female (ANOVA)**

MEASUREMET	P-Value	Sig.
1	<0.01	sig
2	<0.01	sig
3	<0.01	sig
4	<0.01	sig
5	<0.01	sig
6	<0.01	Sig
7	<0.01	sig
8	<0.01	sig
9	<0.01	sig
10	<0.01	sig
11	<0.01	sig
12	<0.01	sig
13	<0.01	sig
14	<0.01	sig
15	<0.01	sig
16	<0.01	sig
17	0.37	not sig
18	<0.01	sig
19	<0.01	sig

### 3.3.4 Differences between anthropometric measurements for male for all year

There are differences in the anthropometric for all measurements (table 9).

**Table 9. Differences of anthropometric measurements by all year for male (ANOVA)**

MEASUREMET	P-Value	Sig.
1	<0.01	Sig
2	<0.01	Sig
3	<0.01	Sig
4	<0.01	Sig
5	<0.01	Sig
6	<0.01	Sig
7	<0.01	Sig
8	<0.01	Sig
9	<0.01	Sig
10	<0.01	Sig
11	<0.01	Sig
12	<0.01	Sig
13	<0.01	Sig
14	<0.01	Sig
15	<0.01	Sig
16	<0.01	Sig
17	0.37	Sig
18	<0.01	Sig
19	<0.01	Sig

### 3.3.5 Difference between anthropometric measurements for male for ages groups 6-11

Table 10 shows that all of the anthropometric measurements are difference significantly between the ages of respondents. These differences would be considered to produce clothing that is appropriate for children of different ages. There are no differences in the anthropometric measurements: 8, 16 and 17. These differences would not be considered in design the clothing sizing systems that are appropriate for children of different age groups. There are differences in the anthropometric for all measurements except arm circumference.

**Table 10. Differences of anthropometric measurements by age groups 6-12 for female (ANOVA)**

MEASUREMET	P-Value	Sig.
1	<0.01	Sig
2	<0.01	Sig
3	<0.01	Sig
4	<0.01	Sig
5	<0.01	Sig
6	<0.01	Sig
7	<0.01	Sig
8	0.26	not sig
9	<0.01	Sig
10	<0.01	Sig
11	<0.01	Sig
12	<0.01	Sig
13	<0.01	sig
14	<0.01	sig
15	<0.01	sig
16	<0.01	sig
17	<0.01	sig

18	<0.01	sig
19	<0.01	sig

19	0.01	Sig
----	------	-----

### 3.3.6 Differences for male for ages groups 12-17

Table 11 shows that all of the anthropometric measurements are difference significantly between the ages of respondents. These differences would be considered to produce clothing that is appropriate for children of different ages. There are no differences in the anthropometric measurement 7.

These differences would not be considered in design the clothing sizing systems that are appropriate for children of different age groups.

There are differences in the anthropometric for all measurements.

## 3.4 Correlation Analysis

A key measurement should also be a body measurement with strong relationships with most other body dimensions. Consequently based on this selection, it was possible to develop sizing system. They can be good predictors of the size of other parts of the body.

The criteria for key measurements vary and there are various methods to be established in this regard. By using correlation coefficients it could be possible to identify key measurements. Correlation coefficient values indicate the strength of linear relationships between variables and were, as such, implemented in this study. Pearson correlation coefficients analysis was carried out to determine the interrelationships between the various body measurements. The following statements explain the strength of the relationship between measurements:

- If correlation coefficient is , 0.5 then no relationship;
- If correlation coefficient is between 0.5 and 0.75 then there is a mild relationship;
- If correlation coefficient is 0.76 it indicates a strong relationship (Gupta and Gangadhar, 2004).

**Table 11. Differences of anthropometric measurements by age groups 12-17 for male (ANOVA)**

MEASUREMET	P-Value	Sig.
1	<0.01	Sig
2	<0.01	Sig
3	<0.01	Sig
4	<0.01	Sig
5	<0.01	Sig
6	<0.01	Sig
7	<0.01	Sig
8	<0.01	Sig
9	<0.01	Sig
10	<0.01	Sig
11	<0.01	Sig
12	<0.01	Sig
13	<0.01	Sig
14	<0.01	Sig
15	<0.01	Sig
16	<0.01	Sig
17	<0.01	Sig
18	<0.01	Sig

### 3.4.1 Correlation analysis for female

It is noted that the weight measurement strong correlation with height and waist circumference. All results for strong relationship between measurements were presented in Table 12.

Additionally front body width has strong with back body width, calf circumference, knee circumference. Additionally back body width has strong with calf circumference and knee circumference. Additionally calf circumference has strong with knee circumference. From these results, it may be concluded that weight measurement is the most critical measurement is shoulder to shoulder length and shoulder to wrist length and shoulder to waist length common to body garments. In general, it can be inferred that these dimensions are the important landmarks on the body and hence should be related closely to the garment measurements.

### 3.4.2 Correlation analysis for male

The results illustrate relationships between measurements and shows the correlation coefficients between each measurement and the other. It is noted that the measurement appears to have strong relationships with other measurements as shown in Table 13. From these findings it may be concluded that measurement is the most critical measurement: height, head circumference, neck circumference are key measurements to body garments. In general, it can be inferred that these dimensions are the important landmarks on the body and hence should be related closely to the garment measurements.

**Table 12. Strong relationship between measurements for female**

Dimensions	Strong relationship
1	5-2
2	8-5
3	8-5-4
4	11-8
5	-
6	7
7	-
8	-
9	19-18-17-16-15-14-13-12-11-10
10	19-18-17-16-15-14-13-12-11
11	19-18-17-16-15-14-13-12
12	19-18-17-16-15-14-13
13	19-18-17-16-15-14
14	19-18-17-16-15
15	19-18-17-16
16	19-18-17
17	19-18
18	19
19	-

**Table 13. Strong relationship between measurements for male**

Dimensions	Strong relationship
1	9-5-2
2	16-14-9-5-4
3	18-16-14-11-9-8-5-4
4	18-14-11-8-5
5	16-14-9-8

6	19-18-7
7	19
8	18-16-14-11
9	16
10	-
11	14
12	-
13	-
14	18-16
15	-
16	-
17	18
18	19
19	-

### 3.5 Regression analysis

Types of regression analysis: There are two types of regression analysis; the first is linear regression, which is the most widespread. Linear regression means that we study the linear relationship. The second type is the nonlinear regression that we need when studying relationships in the form of a curve rather than a straight line.

#### 3.5.1 Results of regression (male)

##### 3.5.1.1 Key dimension 1

$$y = -74 - 2.4 x_1 - 3.54 x_2 + 10.6 x_3 + 0.71 x_4 + 3.37 x_5$$

where;

Y=height,

x1=neck circumference,

x2=waist circumference,

x3=shoulder to shoulder length,

x4=waist to hips length,

x5=front body width.

##### 3.5.1.2 Key dimension 2

$$y = 38.5 + 0.100 x_1 - 0.152 x_2 + 0.500 x_3 + 0.394 x_4 - 0.0256$$

$$x_5 - 0.0730 x_6$$

$$0.129 x_7 + 0.0973 x_8$$

Where,

Y= head circumference,

x1= neck circumference,

x2= waist circumference,

x3=arm circumference,

x4= shoulder to shoulder length,

x5=shoulder to waist length,

x6= waist to hips length,

x7= front body width,

x8=calf circumference.

##### 3.5.1.3 Key dimension 3

$$y = 7.27 + 0.032 x_1 + 0.199 x_2 + 0.101 x_3 - 0.016 x_4 + 0.417$$

$$x_5$$

where,

Y= neck circumference,

x1= waist circumference,

x2= arm circumference,

x3= shoulder to waist length,

x4= waist to hips length,

x5= calf circumference

#### 3.5.2 Results of regression (female)

##### 3.5.2.1 Key dimension 1

$$y = 111 - 1.09 x_1 - 0.638 x_2 - 0.428 x_3 + 2.32 x_4 + 0.48 x_5 -$$

$$1.18 x_6 - 0.320 x_7 + 0.028 x_8$$

Where;

y== shoulder to waist length,

x1=front body length,

x2=back body length,

x3= waist to hips length,

x4=shoulder length,

x5=front body width,

x6=back body width,

x7= calf circumference,

x8=knee circumference.

##### 3.5.2.2 Key dimension 2

$$y = -39.6 + 0.127 x_1 + 0.573 x_2 + 0.165 x_3 + 0.560 x_4 + 0.57$$

$$x_5 - 0.02 x_6 + 0.199 x_7 + 0.710 x_8 + 0.296 x_9$$

Where;

y=shoulder to wrist length,

x1== shoulder to waist length,

x2=front body length,

x3=back body length,

x4= waist to hips length,

x5=shoulder length,

x6=front body width,

x7=back body width,

x8= calf circumference,

x9=knee circumference.

##### 3.5.2.3 Key dimension 3

$$y = 41.1 + 0.859 x_1 - 0.037 x_2 - 0.362 x_3 - 0.135 x_4 - 0.726$$

$$x_5 - 0.554 x_6 - 0.016 x_7 + 0.001 x_8 + 0.167 x_9 - 0.260 x_{10}$$

Where;

Y= shoulder to shoulder length,

x1=shoulder to wrist length,

x2== shoulder to waist length,

x3=front body length,

x4=back body length,

x5= waist to hips length,

x6=shoulder length,

x7=front body width,

x8=back body width,

x9= calf circumference,

x10=knee circumference.

### 3.6 Principle component analysis

Principal component analysis (PCA) is a mathematical procedure that transforms a number of (possibly) correlated variables into a (smaller) number of uncorrelated variables called principal components. The results of principle component analysis show in tables (Table 14 and Table 15 below for male and female).

**Table 14. Principal component analysis for male**

Variable	PC1	PC2	PC3
M1	-0.144	-0.357	-0.104
M2	-0.242	-0.262	-0.018
M3	0.313	0.083	0.003
M4	0.317	0.014	-0.013
M5	-0.236	-0.255	-0.088
M6	0.226	-0.262	-0.182
M7	0.151	-0.296	-0.322
M8	0.306	0.023	-0.048
M9	-0.191	-0.299	-0.051

M10	0.013	-0.366	0.146
M11	0.250	0.024	-0.205
M12	0.197	-0.102	0.589
M13	0.032	-0.297	0.628
M14	0.310	0.006	-0.005
M15	0.228	-0.183	0.004
M16	-0.256	-0.184	-0.083
M17	0.226	-0.188	-0.030
M18	0.272	-0.194	-0.081
M19	0.146	-0.335	-0.143

**Table 15. Principal component analysis for female**

Variable	PC1	PC2	PC3
F1	0.027	0.312	0.447
F2	0.006	0.421	0.092
F3	0.011	-0.428	0.095
F4	0.015	-0.392	0.178
F5	0.024	0.381	0.274
F6	0.130	-0.068	0.599
F7	0.158	-0.146	0.49
F8	0.129	-0.384	0.104
F9	0.288	0.115	-0.032
F10	0.286	0.096	0.049
F11	0.283	-0.114	-0.03
F12	0.295	0.026	-0.079
F13	0.280	0.081	-0.155
F14	0.289	-0.115	-0.048
F15	0.301	-0.005	-0.086
F16	0.290	0.114	-0.107
F17	0.295	0.023	-0.076
F18	0.304	-0.001	-0.051
F19	0.303	0.028	-0.04

	9	20.87	34.07	47.27			
	10	19.35	39.47	59.59			
	11	22.24	46.52	70.80			
2	6	105.44	116.87	128.30			
	7	113.67	125.08	136.49			
	8	113.85	125.01	136.18			
	9	122.30	138.55	154.80			
	10	131.24	143.17	155.09			
3	6	46.85	51.76	56.67			
	7	48.93	52.82	56.72			
	8	48.63	52.68	56.73			
	9	48.77	53.30	57.83			
	10	50.54	54.10	57.66			
4	6	23.13	27.18	31.23			
	7	23.14	28.29	33.44			
	8	24.21	28.13	32.04			
	9	23.37	29.00	34.63			
	10	13.87	32.45	51.03			
5	6	44.92	69.49	94.06			
	7						
	8						
	9						
	10						
		male			Female		
		s	m	l	S	m	l
5	6				49.78	60.90	72.02
	7				51.01	61.18	71.35
	8				49.63	6.01	73.66
	9				51.42	6.71	78.25
	10				48.26	10.77	91.34
11				48.82	9.47	86.71	

**3.7 Development of Size Charts**

The development of the size chart was carried out using values obtained from the statistical information based on the ANOVA test of body dimensions. The mean values and the standard deviations were used for creating size steps for the size chart. Therefore, different sizes of clothing for female and male aged 6 to 17 years must be developed due to the differences in some measurements between age groups three sizes were developed: S (small), M (medium) and L (large).

These sizes were developed because of there were multiple body shape in each group of 6 to 17 years old (as shown in Table 16 and 17). There is a difference between ages in height measurement and most of the measurements based on ANOVA analysis. One of the values can be calculated if there is no difference between each parameter. However, three values can be calculated if there is difference between each parameter according to ANOVA.

**Table 16. Size chart for age groups 6 to 11.**

Measurements	Grade	Male and female		
		S	M	L
1	6	10.01	22.62	35.23
	7	16.58	26.41	36.25
	8	14.71	27.41	40.11

**Table 16. cont.**

Measurements	Grade	Male and female					
		S			L		
6	6	53.56	63.67	73.79			
	7	53.27	62.76	72.25			
	8	52.19	65.13	78.06			
	9	45.95	67.93	89.92			
	10	53.31	69.90	86.49			
11	54.55	75.45	96.35				
		male			Female		
		S	m	l	S	m	l
7	6	61.34	68.00	75.53	50.07	66.30	82.53
	7	55.59	65.21	74.83			
	8	54.93	70.82	86.71			
	9	46.32	64.00	81.68			
	10	48.05	69.68	91.32			
11	47.72	74.03	100.35				
		male and female					
		s		M	l		
8	6	16.02	22.46	28.90			
	7						
	8						
	9						
10							

		11			
		male and female			
		s	M	l	
9	6	26.19	35.64	45.09	
	7				
	8				
	9				
	10				
	11				
		male and female			
		male and female			
		s	M	l	
10	6	28.14	43.22	58.30	
	7				
	8				
	9				
	10				
	11				
		male and famel			
		s	M	l	
11	6	18.81	36.05	53.28	
	7				
	8				
	9				
	10				
	11				

14	6	9.02	15.79	22.55	
	7				
	8				
	9				
	10				
	11				
		male and female			
		s	M	l	
15	6	4.35	12.28	20.20	
	7				
	8				
	9				
	10				
	11				
		male and female			
		s	M	l	
16	6	23.62	32.47	41.32	
	7				
	8				
	9				
	10				
	11				

Table 16. cont.

Measurements	Grade	Male and female					
		S		M		L	
12	6	21.54		37.14		52.74	
	7						
	8						
	9						
	10						
	11						
		male			Female		
		s	m	l	S	M	l
13	6	17.99	23.00	24.61	26.38	45.57	64.76
	7	14.12	37.37	60.61			
	8	26.18	41.10	56.02			
	9	34.16	39.90	45.64			
	10	35.64	41.25	46.86			
	11	33.63	41.03	48.43			
		male and female					
		s	M		l		

Table 16. cont.

Measurements	Grade	Male			Femle		
		S	M	L	S	M	L
17	6	26.37	30.00	32.06	16.80	30.58	44.36
	7	24.60	32.30	40.01			
	8	24.43	33.32	42.22			
	9	22.74	27.83	32.93			
	10	22.80	31.57	40.33			
	11	23.07	30.63	38.20			
18	6	22.31	23.00	25.44	19.51	27.23	34.95
	7	22.91	25.13	27.36			
	8	23.01	24.77	26.54			
	9	19.84	26.37	32.89			
	10	21.30	30.20	39.10			
	11	22.37	32.23	42.10			

19	6	23.91	23.00	28.08	22.44	30.01	37.58
	7	24.47	28.19	31.91			
	8	24.52	27.56	30.59			
	9	22.27	29.93	37.60			
	10	24.52	32.53	40.55			
	11	26.01	34.30	42.59			

**Table 17. size chart for age groups 12 to 17.**

Measurement	Grade	Male and Female		
		S	M	L
1	12	15.58	43.62	71.67
	13	28.53	50.90	73.28
	14	27.23	54.57	81.90
	15	32.69	58.79	84.89
	16	23.07	64.72	106.36
	17	37.36	63.23	89.10
2	12	134.43	148.85	163.27
	13	141.88	156.46	171.03
	14	145.77	162.02	178.26
	15	143.89	163.89	183.89
	16	145.36	166.57	187.78
	17	146.48	167.88	189.29

**Table 17. cont.**

Measurement	Grade	Male and Female		
		S	M	L
3	12	50.66	54.55	58.43
	13	49.70	54.62	59.54
	14	50.00	55.95	61.90
	15	50.54	55.42	60.29
	16	51.13	55.88	60.64
	17	51.14	56.34	61.53
4	12	23.83	29.83	35.83
	13	26.16	31.32	36.47
	14	27.41	32.65	37.90
	15	25.80	35.63	45.46
	16	26.48	36.16	45.84
	17	28.39	36.95	45.51
5	12	42.64	70.59	98.53
	13	56.14	74.23	92.32

	14	56.46			75.06		93.67
	15	62.27			80.25		98.23
	16	61.97			82.33		102.69
	17	61.47			83.48		105.48
		male			female		
		s	m	l	S	m	l
6	12	67.73	77.77	87.82	39.85	69.54	99.22
	13	63.76	80.41	97.05	64.86	82.50	100.14
	14	60.79	79.78	98.77	61.55	82.60	103.64
	15	63.37	81.23	99.10	63.70	86.09	108.47
	16	64.39	84.15	103.91	73.26	87.78	102.30
	17	67.28	83.67	100.05	70.74	91.42	112.09
7	12	47.52	76.69	105.86	48.14	77.63	107.13
	13	66.10	87.20	108.29	72.76	90.58	108.40
	14	69.90	91.65	113.40	64.84	90.80	116.76
	15	54.26	75.30	96.34	74.91	97.30	119.68
	16	48.95	75.27	101.58	62.65	94.12	125.59
	17	54.40	75.27	96.14	68.73	99.41	130.08

**Table 17. cont.**

Measurement	Grade	male			female		
		s	m	l	S	m	l
8	12	20.81	26.57	32.33	14.16	23.67	33.17
	13	19.21	27.61	36.01	20.96	25.98	31.01
	14	19.99	27.44	34.89	20.86	26.76	32.67
	15	18.88	25.37	31.85	21.76	27.56	33.37
	16	18.22	26.40	34.58	21.80	27.43	33.06
	17	18.33	25.90	33.47	11.86	30.24	48.61
		male and female					
		s		M	l		
9	12	32.55		38.72	44.89		
	13	30.98		38.32	45.66		
	14	30.7		39.61	48.52		
	15	30.7		42.46	50.22		

	16	34.69			42.46		50.22	
	17	34.42			43.2		51.98	
		male			Female			
		s	m	L	S	M	L	
10	12	49.2 1	54.5 3	59.8 5	43.0 2	53.2 9	63.5 6	
	13	46.6 0	56.0 9	65.5 7	45.5 7	52.4 6	59.3 4	
	14	55.1 1	61.6 2	68.1 3	45.7 2	55.6 3	65.5 4	
	15	52.7 0	57.0 3	61.3 6	46.3 9	52.4 2	58.4 5	
	16	51.6 6	56.0 2	60.3 8	45.7 1	53.1 6	60.6 0	
	17	49.7 6	55.9 7	62.1 7	36.2 0	51.9 8	67.7 5	
			male			Female		
		s	m	l	s	m	L	
11	1	30.	40.	50.	26.	34.	41.	
	2	17	30	42	93	18	44	
	1	25.	29.	34.	26.	34.	42.	
	3	24	69	14	28	54	80	
	1	20.	38.	56.	20.	35.	51.	
	4	10	18	27	21	76	30	
	1	37.	43.	50.	31.	35.	40.	
	5	82	97	11	26	78	30	
	1	36.	44.	52.	31.	36.	40.	
	6	50	42	33	53	24	94	
1	40.	47.	53.	27.	37.	48.		
7	92	40	88	14	88	62		

Table 17. cont.

Measurement	Grade	male			female		
		s	m	l	s	m	l
12	12	31.2 6	34.6 1	37.9 6	25.1 7	32.2 5	39.3 3
	13	30.0 6	34.7 0	39.3 4	26.1 5	34.0 8	42.0 0
	14	27.6 1	37.8 9	48.1 6	28.3 0	35.9 8	43.6 6
	15	34.1 1	38.3 7	42.6 2	25.8 1	30.9 7	36.1 2
	16	31.0 6	38.5 0	45.9 4	24.2 1	33.0 8	41.9 4
	17	33.4 2	39.4 2	45.4 1	23.4 2	31.7 9	40.1 6
		male			female		
		s	m	l	s	m	l
13	12	35.3 7	42.5 7	49.7 8	28.7 5	35.4 9	42.2 3

	13	28.4 1	44.4 1	60.4 1	28.3 2	35.8 5	43.3 8
	14	38.0 0	49.0 9	60.1 8	29.8 6	37.2 0	44.5 5
	15	44.1 0	53.3 3	62.5 7	40.0 2	45.4 0	50.7 7
	16	43.8 7	53.6 7	63.4 7	37.6 8	44.4 1	51.1 3
	17	47.0 6	53.5 5	60.0 4	33.3 9	44.1 5	54.9 1
		male			female		
		s	m	l	s	m	l
14	12	21.1 8	27.5 2	33.8 5	18.2 0	24.5 2	30.8 4
	13	18.0 0	23.8 8	29.7 6	13.0 1	17.4 7	21.9 3
	14	18.3 9	26.2 6	34.1 2	19.1 0	22.4 0	25.6 9
	15	14.9 7	17.1 3	19.3 0	12.5 1	17.0 5	21.5 8
	16	14.8 2	16.6 3	18.4 5	6.70	17.7 8	28.8 7
	17	14.6 1	16.8 2	19.0 2	7.07	18.9 7	30.8 6
			male and female				
		s		M		l	
15	12	9.73		13.4		17.07	
	13	10.66		14.73		18.8	
	14	7.65		14.7		21.74	
	15	10.81		15.12		19.44	
	16	8.77		14.57		20.38	
	17	7.94		15.6		23.26	
		s		M		l	
16	12	28.24		36.36		44.48	
	13	28.78		35.21		41.63	
	14	26.8		35.2		43.61	
	15	28.06		37.53		47.01	
	16	26.21		35.97		45.73	
	17	26.56		37.67		48.78	

Table 17. cont.

Measurement	Grade	male and female			
		s	M	l	
17	12	18.63	38.17	57.72	
	13				
	14				
	15				
	16				
	17				
		male		female	

		s	m	l	s	m	l
18	12	26.6 5	31.3 5	36.0 5	19.5 8	30.7 2	41.8 7
	13	24.8 0	33.9 5	43.1 1	28.0 1	33.6 4	39.2 8
	14	27.5 0	36.2 0	44.9 0	27.2 8	33.5 9	39.9 0
	15	27.1 4	35.7 8	44.4 3	28.2 2	34.9 2	41.6 3
	16	26.0 2	35.0 3	44.0 5	30.0 5	34.9 1	39.7 7
	17	25.1 5	34.7 2	44.2 8	28.9 3	36.0 9	43.2 5
		male			female		
		s	m	l	s	m	l
19	12	30.2 7	35.1 6	40.0 5	36.9 0	44.9 7	53.0 3
	13	31.0 3	38.2 6	45.4 8	33.9 4	42.0 9	50.2 4
	14	26.9 5	36.2 6	45.5 6	36.7 1	45.0 0	53.2 9
	15	30.0 8	36.6 2	43.1 6	31.3 6	38.5 7	45.7 7
	16	15.9 8	37.6 0	59.2 2	30.2 6	39.8 1	49.3 5
	17	28.5 0	35.8 8	43.2 6	29.2 4	36.2 7	43.2 9

#### 4. CONCLUSION

The following conclusions were derived

1. As expected that all measurements follow a normal distribution.
  2. The ANOVA test was used to find the differences between age groups. From the results of these tests, there were differences of anthropometric measurements between age groups for females (ages group from 6 to 11), except hip circumference, arm circumference, back body width, calf circumference and knee circumference are no significant differences. However, most of measurements are significant difference except back body width for age group 12 to 17. For male students, all measurements are significant differences except arm circumference (age group 6-11). However, there are no significant differences between age groups (12-17) for all measurements (male students).
  3. The key dimensions should be those which have the strongest correlations with most other body dimensions. From the results, it can be concluded that Height, Head circumference and Neck circumference is very strongly correlated with some of dimensions for male students. Moreover, Shoulder to Shoulder length, shoulder to wrist length, and shoulder to waist length are key dimensions for female students. In general, it can be inferred that these dimensions are the important landmarks on the body and hence should be related closely to the garment measurements.
- In conclusion, the main aspect that needs to be seen by an apparel manufacturer is clothing size. They need to know the exact size before producing their clothes. Thus, the development of sizes should be according to their procedure in order to produce an accurate size that fits the consumer's body, especially children.

#### 5. ACKNOWLEDGMENTS

This study is a part of a BSc. project conducted at School of Industrial and Manufacturing Systems Engineering at University of Benghazi in Fall 2018-2019. The authors would like to thank all participants for their contributions.

#### 6. REFERENCES

- [1] Adu-Boakye, S., Power, J., Wallace, T., Chen, Z. (2012) Development of a Sizing System for Ghanaian Women for the Production of Ready-To-Wear Clothing. In: The 88th Textile Institute World Conference 2012, 15th-17th May 2012, Selangor, Malaysia.
- [2] Ariadurai, A. S., Nilusha, T. P. G. and Dissanayake, M. R. 2009. An anthropometric study on Sri Lankan school children for developing clothing sizes, Journal of Social Science, 19, 51– 56.
- [3] Alarody, I.; Kared, M.; Abdelmalek, S.; An anthropometric study to develop clothing charts for Benghazi school children; B.Sc. Project, Industrial and Manufacturing Systems Engineering Department; University of Benghazi; Fall 2015/2016.
- [4] Albarki, F.; Bu-Hager, A.; Basheer, M. and Ali, M.; An anthropometric study to develop clothing charts for seventh, eighth and ninth grades of benghazi school children b.Sc. Project, Industrial and Manufacturing Systems Engineering Department; University of Benghazi; Spring 2016/2017.
- [5] Bilhassan\*, S.; Albarki, F.; Bu-Hager, A.; Basheer, M.; Ali M.; 2018(a); An anthropometric study to develop clothing charts for seventh, eighth and ninth grades of Benghazi schoolchildren; Libyan Journal of Science & Technology vol. 7, No. 2
- [6] Bilhassan, S; ELMABROK, A; ELMHASHHSH, K; Ali, H; Kaddom, A; Elhouni, H; 2018 (b); Development of A Clothing Sizing System for Benghazian Children Based on Anthropometric Measurements; The International Journal of Engineering and Information Technology), Vol.4, No.2.
- [7] Bilhassan, S., Ali, H., Boushagour, H., Mohmed, H., Alobaidy, N., Development of a Clothing Sizing System for Benghazian School Girls Students Based on Anthropometric Measurements. International Journal of Science and Engineering Applications Volume 9–Issue 03, 31-35, 2019, ISSN:-2319–7560 www.ijsea.com 31
- [8] Boushagour, H.; Alobaidy, N.; Ali, H.; Mohammed, H.; An anthropometric study to develop clothing sizing system for Benghazi school girl students based on Anthropometric measurement; B.sc Project, Industrial and manufacturing system Engineering Department; University of Benghazi; Fall 2017/1018.
- [9] Chan, A.C.K., 2014. The development of apparel sizing systems from anthropometric data. In Anthropometry, Apparel Sizing and Design (pp. 167-196).
- [10] Dawal,S., Zadry, H., Syed Azmi, S., Rohim, S.; Sartika, S.; 2012; Anthropometric database for the learning environment of high school and university students. Int. J. Occup. Saf. Ergon., 18 (4), pp. 461-472.
- [11] Elmabrouk, A.; Elmehashhash, K.; Ali, H.; Kaddom, A.; Elhouni, h.; An anthropometric study to develop clothing charts for Benghazi school children B.Sc. Project,

Industrial and Manufacturing Systems Engineering Department; University of Benghazi; Fall 2016/2017.

- [12] Elurfi, A.; Abdelsalam, A.; Mohamed, H.; Alammari, M.; Develop Clothing Charts for Fifteenth, Sixteenth and Seventeenth Grades of Benghazi School Children; B.sc Project, Industrial and manufacturing system Engineering Department; University of Benghazi; Spring 2017/1018.
- [13] Gupta, D., Zakaria, N., Anthropometry, apparel sizing and design, Woodhead Publishing Limited in association with The Textile Institute, UK, 2014.
- [14] Gupta, D., 2014. Anthropometry and the design and production of apparel: an overview. In *Anthropometry, Apparel Sizing and Design* (pp. 34-66).
- [15] Gupta, D. and Gangadhar, B.R., 2004. A statistical model for developing body size charts for garments. *International Journal of Clothing Science and Technology*, 16(5), pp.458-469.
- [16] Qutubuddin SM, Hebbal SS, and Kumar ACS. 2012. Significance of anthropometric data for the manufacturing organizations. *Int J Eng Res Indus Appl* 5(I):111–26.
- [17] Shiru, J., Abubakar, S., 2012; Anthropometry in engineering design (a case study of cassava grating machines installed in Doko and Kutigi metropolis of Lavun local government areas of Niger state) *Niger. Acad. Forum*, 22 (1), pp. 132-139.
- [18] Veitch, D., Veitch, L. and Henneberg, M., 2007. Sizing for the clothing industry using principal component analysis—an Australian example. *Journal of ASTM International*, 4(3), pp.1-12.
- [19] Viviani, C., P. M. Arezes, S. Bragança, J. Molenbroek, I. Dianat, and H. I. Castellucci. 2018. “Accuracy, Precision and Reliability in Anthropometric Surveys for Ergonomics Purposes in Adult Working Populations: A Literature Review.” *International Journal of Industrial Ergonomics* 65: 1–16.
- [20] Widyanti, A., Mahachandra, M., Soetisna, H.R. and Sitalaksana, I.Z., 2017. Anthropometry of Indonesian Sundanese children and the development of clothing size system for Indonesian Sundanese children aged 6–10 year. *International Journal of Industrial Ergonomics*, 61, pp.37-46.
- [21] Xia, S. and Istook, C., 2017. A Method to Create Body Sizing Systems. *Clothing and Textiles Research Journal*, 35(4), pp.235-248.
- [22] Zakaria, N. and Gupta, D., 2014. Apparel sizing: existing sizing systems and the development of new sizing systems. In *Anthropometry, Apparel Sizing and Design* (pp. 3-33).
- [23] Zakaria, N., 2014. Body shape analysis and identification of key dimensions for apparel sizing systems. In *Anthropometry, Apparel Sizing and Design* (pp. 95-119)

# A Vehicle and Pedestrian Detection Method Based on Improved YOLOv4-Tiny

Hui Xiang  
College of Electromechanical  
Engineering  
Qingdao University of Science  
and Technology  
Qingdao, China

Junyan Han  
College of Electromechanical  
Engineering  
Qingdao University of Science  
and Technology  
Qingdao, China

Hanqing Wang  
College of Electromechanical  
Engineering  
Qingdao University of Science  
and Technology  
Qingdao, China

Hao Li  
College of Electromechanical  
Engineering  
Qingdao University of Science  
and Technology  
Qingdao, China

Shangqing Li  
College of Electromechanical  
Engineering  
Qingdao University of Science  
and Technology  
Qingdao, China

Xiaoyuan Wang  
College of Electromechanical  
Engineering  
Qingdao University of Science  
and Technology  
Qingdao, China

**Abstract:** Aiming at the problems of low detection accuracy and poor recognition effect of small-scale targets in traditional vehicle and pedestrian detection methods, a vehicle and pedestrian detection method based on improved YOLOv4-Tiny is proposed. On the basis of YOLOv4-Tiny, the 8-fold down sampling feature layer was added for feature fusion, the PANet structure was used to perform bidirectional fusion for the deep and shallow features from the output feature layer of backbone network, and the detection head for small targets was added. The results show that the mean average precision of the improved method has reached 85.93%, and the detection performance is similar to that of YOLOv4. Compared with the YOLOv4-Tiny, the mean average precision of the improved method is increased by 24.45%, and the detection speed reaches 67.83FPS, which means that the detection effect is significantly improved and can meet the real-time requirements.

**Keywords:** computer vision; deep learning; YOLOv4-Tiny; vehicle detection; pedestrian detection

## 1. INTRODUCTION

In recent years, with the continuous improvement of hardware computing performance, the target detection method based on convolutional neural networks (CNN) has become the mainstream because of its strong learning ability. The traditional vision-based target detection methods construct detectors by manually extracting target image features or by machines selecting different target image features. In contrast, the CNN-based method can autonomously and centrally calculate the multi-layer features of the target image, and as the network depth increases, higher-dimensional features will be learned and have better feature expression capabilities for the target. For advanced driving assistance system, the improvement of target detection method will contribute to improve the perception ability of the external environment of the vehicle, so as to make real-time response to the driving road environment.

At present, the target detection methods based on CNN are mainly divided into two categories. One is a two-stage target detection algorithm and the detection process is divided into two steps: generating candidate regions and extracting image features of candidate regions for classification and regression. The typical algorithms are: R-CNN [1], Fast-RCNN [2], Faster R-CNN [3], R-FCN [4] and Mask R-CNN [5]. Limited by the complex network structure, the real-time performance of the two-stage method is not enough for practical application. The other is one-stage target detection method. The target location and category are classified and regressed by a single network, which takes into account the detection

speed and accuracy. The typical algorithms include SSD [6], DSSD [7], YOLO [8], YOLOv2 [9], YOLOv3 [10] and YOLOv4 [11].

In order to realize the timely and accurate detection of vehicles and pedestrians in front under the complex driving road environment, YOLOv4-Tiny [11] is used as the basis to improve the network structure and the detection accuracy while ensuring the detection speed, so as to meet the actual needs of the driving environment.

## 2. INTRODUCTION TO YOLOV4-TINY

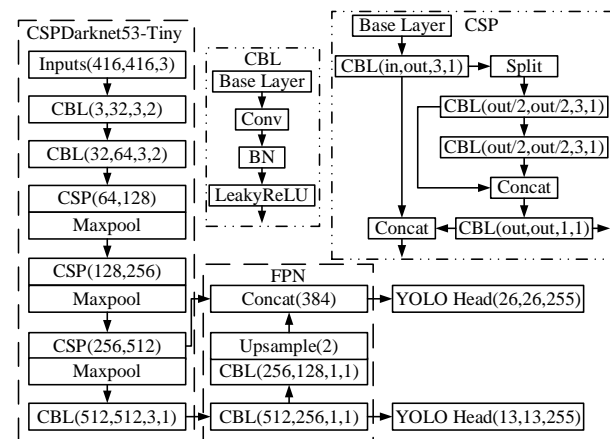


Figure 1. Network structure of YOLOv4-Tiny

In April last year, YOLOV4 was proposed on the basis of YOLOv3, and its detection speed and detection rate have been improved. YOLOv4-Tiny is a lightweight version of YOLOv4. Compared with YOLOv4, the network structure of YOLOv4-Tiny is simpler, the detection speed is faster, and it performs well in the target detection algorithm. The network structure of YOLOv4-Tiny is shown in Figure 1.

As we can see in Figure 1, CSPDarknet53-Tiny is used as the backbone for YOLOv4-Tiny, which mainly includes Convolution Block (CBL), Cross Stage Partial Connections (CSP) and down sampling module. CBL is composed of ordinary convolution (Conv), batch normalization layer (BN), and activation function (Leaky ReLU). In CSP, after the input feature is convolved with a convolution kernel size of  $3 \times 3$  and a step size of 1, the convolution result  $X$  is obtained. Then the features obtained by result  $X$  passing through CBL twice and CBL once are stacked in the channel dimension, and the result after stacking is named as  $Y$ . Finally, the result  $Y$  is convolved with  $1 \times 1$  convolution to increase the nonlinear expression ability of the network, and the result after convolution is named as  $Z$ . The result  $Z$  can be selected as the input of the feature fusion part. The result  $X$  and  $Z$  are stacked in the channel dimension as the output of the CSP. Max pooling is chosen as the down sampling module. Feature pyramid network (FPN) is chosen to be the feature fusion part of YOLOv4-Tiny, which can fuse the  $13 \times 13$  feature layer output by the backbone network with the  $26 \times 26$  feature layer to improve feature extraction capabilities. Finally, Yolo head is used to perform target regression and classification on the feature layer coming from FPN.

### 3. IMPROVEMENT OF YOLOV4-TINY

The simple network structure of YOLOv4-Tiny is not enough to learn sufficient vehicle and pedestrian characteristics. Based on the original YOLOv4-Tiny, a real-time lightweight vehicle detection model is designed, which can reduce the false and missed detection in vehicle and pedestrian detection and improve the detection performance.

With the continuous deepening of the backbone network level, the resolution of the feature layer continues to decrease, and the semantic dimension continues to deepen. The shallow features have a higher resolution and contain more regional texture details, which are suitable for determining the location of the target. The deep features contain higher-dimensional regional semantic information and are suitable for target classification. In the feature fusion part, the original YOLOv4-Tiny only selected two different scale features of  $13 \times 13 \times 512$  and  $26 \times 26 \times 256$  in the backbone as the input of FPN, so that the network contains both high-dimensional semantic information and low-dimensional texture details. With this fusion strategy, feature information of different scales is less fused, the model is not sensitive to targets of different sizes, and the detection accuracy of the model is low. For this reason, on the basis of the original backbone network output, the  $52 \times 52 \times 128$  shallow feature layer output by the second CSP convolutional layer in CSPDarknet53-Tiny, which is the 8-fold down sampling feature layer of the input image, is added as the input of the feature fusion part.

In addition, through the feature fusion strategy of bottom-up and top-down, the Path Aggregation Network (PANet) is used to perform bidirectional fusion for the deep and shallow features from the output feature layer of backbone network. Therefore, three scale feature maps of  $13 \times 13 \times 512$ ,  $26 \times 26 \times 256$  and  $52 \times 52 \times 128$  are output to form the final feature expression. Finally, the feature maps of three scales are respectively used to output the prediction results through three convolutional layers with the same number of channels. And the number of channels in the convolutional layer is set to  $(5+3) \times 3 = 24$ . Above all, based on YOLOv4-Tiny, the improved network called YOLOv4-Tiny-DL3 has been constructed, and its specific network structure is shown in Figure 2.

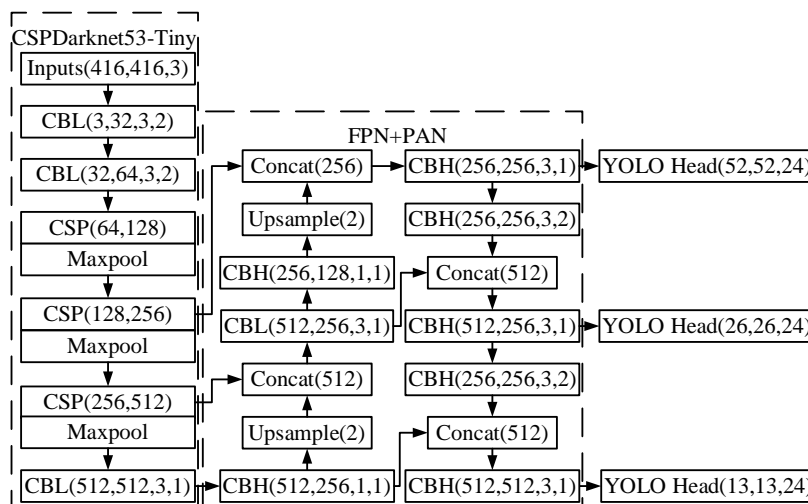


Figure 2. Network structure of YOLOv4-Tiny-DL3

## 4. EXPERIMENT AND ANALYSIS

### 4.1 Dataset

In the experiment, the KITTY dataset is selected as the vehicle and pedestrian detection dataset. The KITTY training

set has 7481 pictures. Since the KITTY test set has no labeled information, the KITTY training set is redivided as the training set and validation set of this article according to the ratio of 9:1. The original dataset annotation file includes nine

category labels. In this paper, the original “Truck”, “Van”, “Tram” and “Car” tag categories are merged into “Car”; the original “Pedestrian” and “Person\_sitting” tag categories are merged into Person; the original “Cyclist” tag category is retained, and the other two tag categories are eliminated. Next, the annotation file is transformed from the original KITTY dataset format to the VOC format. As a result, the annotation files required for the dataset in this article are obtained. The number of categories in the divided training set and test set is shown in the figure below.

**Table 1. Number of categories in datasets**

	<b>Car Number</b>	<b>Person Number</b>	<b>Cyclist Number</b>
Training set	30079	4251	1481
Verification set	3182	458	416

## 4.2 Experimental platform

The hardware platform selected in this paper is as follows: the system processor is Intel(R)Core(TM)i7-10870H CPU @2.20GHz, the memory is 16G, the operating system is ubuntu18.04, the deep learning framework is Pytorch1.7, the model parallel computing framework is CUDA 11.1, and the model acceleration library is CUDNN 8.0.5.39.

## 4.3 Experimental setup

During training, the input image size of each model is 416×416, the input batch size is 8, and the training epoch is 300. The COCO pretraining model was used for the first 50 epoch, and the model parameters are adjusted by freezing the

backbone network. The initial learning rate is set to 0.001; the cosine annealing learning method is used later to gradually reduce the learning rate from 0.001 to 0.0001. The prior boxes used during training are: (8, 11), (13, 25), (28,1 9); (25, 51), (52, 28), (49, 38); (97, 75), (131, 166), (314, 274). During training, the loss function used in the paper is the same as YOLOv4.

## 4.4 Experimental result

Model detection performance is evaluated based on Precision (P), Recall (R), mean Average Precision (mAP), and FPS. FPS is used to measure the detection efficiency, which represents the number of images that the model can process per second. The mAP value is defined as the mean value of the average precision (Average Precision, AP) of each class, and the AP value corresponds to the area under a certain type of P-R curve. The calculation formulas are shown as follows.

$$Precision = \frac{TP}{TP + FP} \quad (1)$$

$$Recall = \frac{TP}{TP + FN} \quad (2)$$

$$AP = \int_0^1 PdR \quad (3)$$

Among them, TP means that the prediction box matches the label box correctly; FP means that the background is predicted to be an object; FN means that the object is predicted to be the background.

**Table 2. Model performance comparison table**

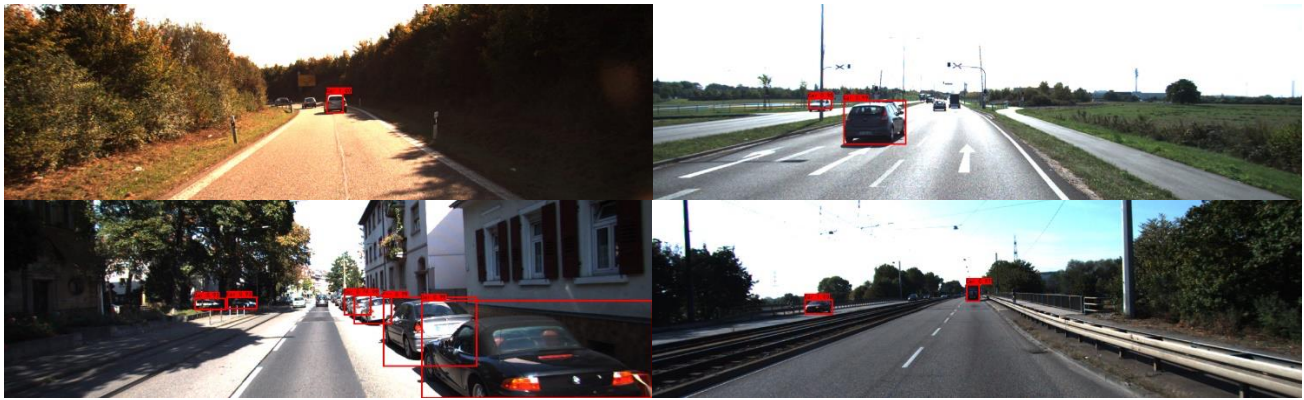
<b>Models</b>	<b>AP/%</b>			<b>mAP/%</b>	<b>Parameters/M</b>	<b>BFLOPs</b>	<b>FPS</b>
	<b>Car</b>	<b>Person</b>	<b>Cyclist</b>				
YOLOv4-Tiny	86.79	57.22	63.15	69.05	6.06	3.47	79.75
YOLOv4-Tiny-DL3	95.88	75.64	86.58	85.93	12.67	8.93	67.83
YOLOv4	95.80	76.78	88.35	86.98	63.95	29.89	30.13

Table 2 shows the experimental results of YOLOv4-Tiny, YOLOv4 and YOLOv4-Tiny-DL3 proposed in this paper. The experimental results are all obtained from training set and testing set selected from the KITTY dataset. It can be seen from the table that the YOLOv4-Tiny-DL3 model is improved by the YOLOv4-Tiny model, and its detection effect is better after the improvement; the AP value of Car has increased by 9.09, the AP value of Person has increased by 18.42, the AP value of Cyclist has increased by 23.43 and the overall mAP value has increased from 69.05 to 85.93. It can be confirmed that the fused multi-scale feature map contains more useful information owing to the 8-fold down-sampling feature layer is added for feature fusion in the YOLOv4-Tiny-DL3 model. In addition, the added small target detection head and PAN feature fusion strategy are beneficial for small target detection. The improved model has a small increase in network parameters. Although the FPS has dropped to a certain extent, the overall FPS can still reach 67.83, which has high real-time performance.

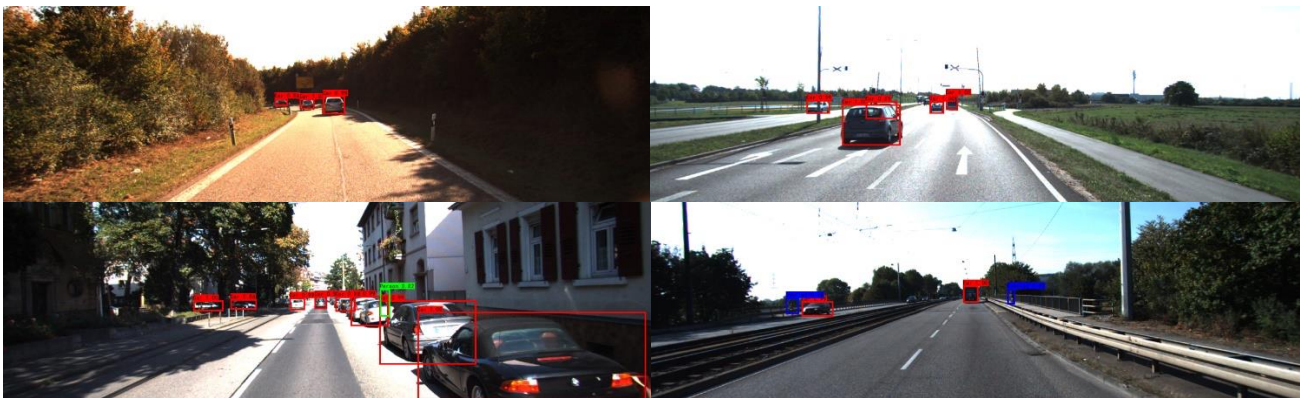
What’s more, compared with the YOLOv4 model, the YOLOv4-Tiny-DL3 model proposed in this paper achieves similar detection performance and more than twice the detection speed with a lower number of model parameters and computational requirements.

## 4.5 Qualitative analysis of results

In order to analyze the experimental results of this paper more intuitively, some results of YOLOv4-Tiny and YOLOv4-Tiny-DL3 on the KITTY dataset are respectively visualized in Figure 3(a) and Figure 3(b) when the input image resolution is 416×416. In the figure, the red detection box refers to the “Car” category; the green detection box refers to the “Person” category; the blue detection box refers to the “Cyclist” category. Compared with YOLOv4-Tiny, YOLOv4-Tiny-DL3 can detect farther "Car" targets. For "Person" targets and "Cyclist" targets with a small proportion of pixels in the image, YOLOv4-Tiny did not detect it, while YOLOv4-Tiny-DL3 can detect it. In summary, YOLOv4-Tiny-DL3 can detect smaller targets, reduce the missed detection rate of



(a) Visual detection results of YOLOv4-Tiny



(b) Visual detection results of YOLOv4-Tiny-DL3

Figure. 3 Comparison of visual detection results between YOLOv4-Tiny and YOLOv4-Tiny-DL3 models

small targets, and have better detection accuracy for small targets.

## 5. CONCLUSION

A vehicle and pedestrian detection method based on improved YOLOv4-Tiny was proposed. Owing to the original YOLOv4-Tiny network only contains two prediction scales of  $13 \times 13$  and  $26 \times 26$ , the model has a good recognition rate for large and medium objects in the image, except for small targets objects. Therefore, the 8-fold down sampling feature layer from the backbone network is used for prediction, and then the feature fusion strategy of PANet is added to fuse the features of three different scales output by the backbone network, which is beneficial to promote the bidirectional fusion of deep features and shallow features. In addition, the detection head for small targets is added to the network to make it more sensitive to small targets, so as to overcome the shortcomings of the original network's lack of small target detection capabilities. Through the improvement of the above method, the overall detection performance of YOLOv4-Tiny-DL3 is improved significantly. Compared with the previous network model, the final mAP value of the YOLOv4-Tiny-DL3 has increased from 69.05 to 85.93 and the FPS of the model has reached 67.83, which has high real-time performance.

## 6. ACKNOWLEDGMENTS

This study was funded by the Qingdao Top Talent Program of Entrepreneurship and Innovation (Grant No.19-3-2-11-zhc), the Natural Science Foundation of Shandong Province (Grant No. ZR2020MF082), the Foundation of Shandong Intelligent Green Manufacturing Technology and Equipment Collaborative Innovation Center (Grant No. IGSD-2020-012), and the National Key Research and Development Project (Grant No.2018YFB1601500).

## 7. REFERENCES

- [1] Girshick R, Donahue J, Darrell T, et al. Rich Feature Hierarchies for Accurate Object Detection and Semantic Segmentation[C]. 2014 IEEE Conference on Computer Vision and Pattern Recognition, 2014: 580-587.
- [2] Girshick R. Fast R-CNN[C]. 15th IEEE International Conference on Computer Vision, ICCV 2015, December 11, 2015 - December 18, 2015, 2015: 1440-1448.
- [3] Ren S, He K, Girshick R, et al. Faster R-CNN: Towards Real-Time Object Detection with Region Proposal Networks[J]. IEEE Transactions on Pattern Analysis and Machine Intelligence, 2017, 39(6): 1137-1149.
- [4] Dai J, Li Y, He K, et al. R-FCN: Object detection via region-based fully convolutional networks[C]. 30th

- Annual Conference on Neural Information Processing Systems, NIPS 2016, December 5, 2016 - December 10, 2016, 2016: 379-387.
- [5] Tian J, Yuan J, Liu H. Road Marking Detection Based on Mask R-CNN Instance Segmentation Model[C]. 2020 International Conference on Computer Vision, Image and Deep Learning, CVIDL 2020, July 10, 2020 - July 12, 2020, 2020: 246-249.
- [6] Liu W, Anguelov D, Erhan D, et al. SSD: Single shot multibox detector[C]. 14th European Conference on Computer Vision, ECCV 2016, October 8, 2016 - October 16, 2016, 2016: 21-37.
- [7] Fu C-Y, Liu W, Ranga A, et al. DSSD : Deconvolutional Single Shot Detector[J]. arXiv e-prints, 2017: arXiv:1701.06659.
- [8] Redmon J, Divvala S, Girshick R, et al. You Only Look Once: Unified, Real-Time Object Detection[C]. 2016 IEEE Conference on Computer Vision and Pattern Recognition (CVPR), 2016: 779-788.
- [9] Redmon J, Farhadi A. YOLO9000: Better, Faster, Stronger[C]. 2017 IEEE Conference on Computer Vision and Pattern Recognition (CVPR), 2017: 6517-6525.
- [10] Redmon J, Farhadi A. YOLOv3: An Incremental Improvement[J]. arXiv e-prints, 2018: arXiv:1804.02767.
- [11] Bochkovskiy A, Wang C-Y, Liao H-Y. YOLOv4: Optimal Speed and Accuracy of Object Detection[M]. 2020.

# Freeze-Thaw Behavior of Stabilized Clayey Soil with Red Mud and Cement

Ekrem Kalkan  
Department of Civil Engineering  
Engineering Faculty  
Ataturk University  
Erzurum, Turkey

**Abstract:** The clayey soils in areas with seasonal frost are exposed to at least one freeze-thaw cycle every year and worsen their engineering properties. To prevent the engineering properties of clayey soils, it is necessary to improve the freeze-thaw resistance of them. In this study, the clayey soil was stabilized by using red mud and cement additive materials. Prepared samples of clayey soil and stabilized clayey soil were subjected to the unconfined compressive test. To investigate the effects of red mud and cement additive materials on the freeze-thaw resistance of clayey soil, the natural and stabilized expansive soil samples were exposed to the freeze-thaw cycles under laboratory conditions. The obtained results showed that the red mud and cement additive materials increased the freeze-thaw resistance of clayey soil. Consequently, it was concluded that red mud and cement additive materials can be successfully used to improve the freeze-thaw resistance of clayey soils.

**Keywords:** Clayey soil, red mud, cement, unconfined compression strength, freeze-thaw

## 1. INTRODUCTION

The clayey soils are generally classified as expansive soils and these soils are known to cause severe damage to structures resting on them. However, these soils are very important in geology, construction, and for environmental applications, due to their wide usage as impermeable and containment barriers in landfill areas and other environmentally related applications (Erguler and Ulusay, 2003; Harvey and Murray, 1997; Kayabali, 1997; Keith and Murray 1994; Murray, 2000; Sabtan, 2005; Kalkan and Akbulut, 2004; Kalkan et al., 2019; Indiramma et al., 2020; Yarbaşı and Kalkan, 2020).

The effects of freeze-thaw cycles on the geotechnical properties of clayey soils were studied (Lee et al., 1995; Eigenbrod, 1996; Konrad, 2000; Simonsen and Isacsson, 2001; Simonsen et al., 2002; Zhang et al., 2004; Kalkan, 2009). It was seen as a reason of such behavior in low freezing rate, pre-consolidation pressure developed during freezing, formation of new bonding between soil fabric units, and changes in free water (Broms and Yao, 1964; Yong et al., 1985; Eigenbrod, 1996; Yang et al., 2003; Kalkan, 2009). These changes are attributed to increased saturation with water caused by freezing and thawing, but much of the increase is attributed to changes in soil structure (Chamberlain et al., 1990; Porebska, 1994; Kalkan, 2009; Yarbaşı and Kalkan, 2021).

When the mechanical qualities of expansive soils are lower than those required, stabilization can be an option to improve performance, notably in enhancing its strength. Improvement of certain desired properties like bearing capacity, shear strength and permeability characteristics of soils can be undertaken by a variety of ground improvement techniques such as densification, reinforcement and stabilization (Kalkan, 2012; Lasaki et al., 2018). Soil improvement techniques can be classified in various ways, for example, mechanical, chemical, and physical stabilization (Ingles and Metcalf,

1977; Lambe and Whitman, 1979; Chen, 1988; Chu et al., 2009; Naeini and Mahdavi, 2009; Manar et al., 2015).

In the mechanical stabilization, the soil density is increased by the application of mechanical forces in the case of surface layer compaction. Chemical stabilization includes incorporation of additives such as natural soils, industrial by-products or waste materials, and cementitious and other chemicals. Physical stabilization includes changing the physical conditions of a soil by means of heating or freezing (Naeini and Sadjadi, 2008; Arab, 2019; Yarbaşı and Kalkan, 2019).

Soil improvement techniques may have the disadvantages of being ineffective and expensive. Therefore, new methods are still being researched to increase the strength properties and to reduce the swell behaviors of clayey soils (Puppala and Musenda, 1998). Many investigators have experienced on natural, fabricated, and by-product materials to use them as additive materials for the modification of clayey soils (Aitcin et al., 1984; Nelson and Miller, 1992; Sandra and Jeffrey, 1992; Asavasipit et al., 2001; Prabakar et al., 2003; Kalkan and Akbulut, 2004; Cetin et al., 2006; Kalkan, 2006; Kalkan, 2011; Kalkan et al., 2020).

The objectives of this research were to investigate the effects of red mud and red mud-cement mixtures on the unconfined compressive strength (UCS) values of clayey soil samples and to test the freeze-thaw resistance of stabilized clayey soil samples with red mud and red mud-cement mixtures. The unconfined compressive strength and freeze-thaw tests were carried out in accordance with related standard procedures to achieve these objectives.

## 2. MATERIAL and METHODS

### 2.1. Clayey Soil

The clayey soil has been supplied from the clay deposits of Oltu Oligocene sedimentary basin, Erzurum, NE Turkey. It is over-consolidated and it has clayey-rock characteristics in

natural conditions. It is defined as a high plasticity soil (CH) according to the Unified Soil Classification System (Kalkan, 2003; Kalkan and Bayraktutan, 2008; Kalkan, 2018; Kalkan et al., 2019). The grain size distribution was given in Figure 1.

## 2.2. Red Mud

Red mud used in this study was provided from Etibank Seydişehir Aluminium Plant, Konya, Turkey. It had a density of 28.5 Mg/m<sup>3</sup> and specific gravity of 3.05. The grain size distribution of red mud was given in Figure 1.

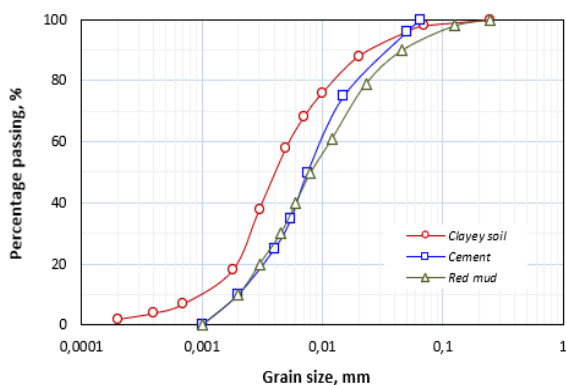


Figure 1. Grain size distribution of clayey soil, red mud and cement

## 2.3. Cement

Cement (PC42.5) used in this study was supplied from a local hardware store in Erzurum, NE Turkey. It had a specific gravity of  $G_s = 8.32 \text{ lb/ft}^3$  ( $3.13 \text{ g/cm}^3$ ), specific surface of  $s = 1496 \text{ ft}^2/\text{lb}$  ( $3063 \text{ cm}^2/\text{g}$ ), and compressive strength of  $\sigma = 59 \text{ MPa}$  ( $590 \text{ kg/cm}^2$ ) at 28 days. The grain size distribution of cement was given in Figure 1.

## 2.4. Sample Preparation

Firstly, clayey soil, red mud and cement were mixed at the required contents under dry condition. Then, amount of optimum water added to the mixtures and blended. The compacted samples were prepared in accordance with Standard Proctor procedure. The samples with 70 mm high and 35 mm diameter subjected to the unconfined compression and freeze-thaw tests.

## 2.5. Unconfined Compressive Test

The unconfined compression tests were carried out in accordance with ASTM 2166. In this test, three cylindrical samples with a 70 mm length and 35 mm diameter were used. The samples were placed in a moist container to prevent from drying while waiting a turn at the compression machine. At least three samples were tested for each combination of variables at a deformation rate of 0.16 mm/min.

## 2.6. Freeze-Thaw Test

The freeze-thaw tests were performed in accordance with ASTM C 666. All samples were placed in the freezing apparatus and conditioned at  $-18 \text{ }^\circ\text{C}$ . After the freezing was completed, the samples were transferred from the freezing apparatus into a test room at  $+20 \text{ }^\circ\text{C}$ . The freeze-thaw cycle was repeated 20 times.

## 3. Results and Discussion

The effects red mud and cement on the clayey soil were illustrated in Figure 2. It is clearly seen that the red mud and

cement played an important role and with the addition of these additives UCS values increased. The effect of the mixtures of red mud-cement on the increase of the UCS value was more than that of the red mud. The increase in the UCS values with the addition of red mud and cement was attributed to the changing composition of the clayey soil. With the addition of red mud and cement to the clayey soil, the particle origin, particle size distribution and surface area of the composite samples changed resulting the increasing in the UCS values (Pera et al., 1997; Attom and Al-Sharif, 1998; Kalkan and Akbulut, 2004; Kalkan, 2006).

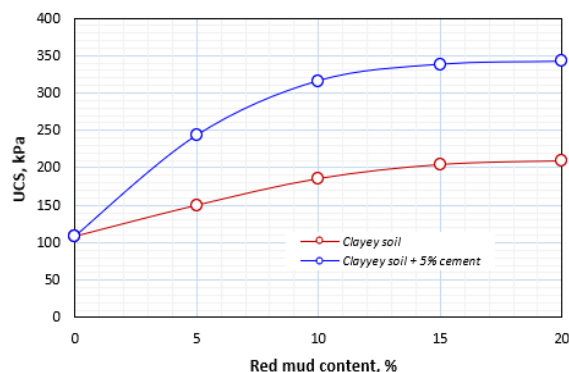


Figure 2. Variation of UCS values with the addition of red mud and cement

To investigate the effects of red mud and cement additive materials on the freeze-thaw resistance of stabilized clayey soil samples, the natural and stabilized clayey soil samples have been subjected to the freeze-thaw cycles. At the end of the freeze-thaw cycles, the natural and stabilized clayey soil samples were tested at the unconfined compression test apparatus under laboratory condition. The effects of the freeze-thaw cycles on the UCS of natural and stabilized fine-grained soil samples were shown in Figure 3.

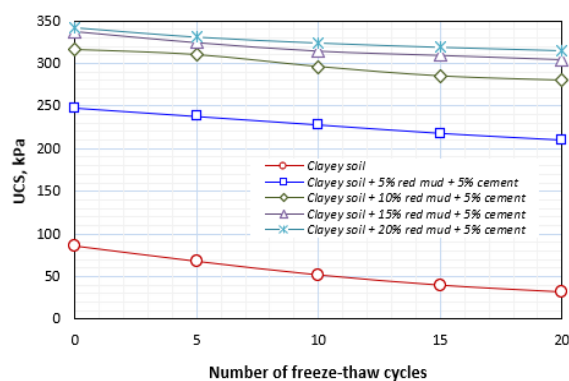


Figure 3. Variation of UCS values with the freeze-thaw cycles

The experimental results show that the red mud and cement additive materials plays a significant role on the freeze-thaw properties of clayey soils. The UCS values of natural and stabilized clayey soil samples are affected by increasing the number of freeze-thaw cycles. However, the red mud and cement additive materials improve the freeze-thaw durability of stabilized clayey soil samples as compared with natural clayey soil samples. The main mechanism governing the alteration of soil behavior caused by the freezing and thawing cycles is believed to be changes in the soil structures

(Eigenbrod et al., 1996; Viklander, 1997; Viklander and Eigenbrod, 2000; Kalkan, 2009).

### 3. CONCLUSIONS

In this study, the effect of red mud and cement additive materials on the freeze-thaw resistance of clayey soil was investigated. The results showed that the red mud and cement additive materials played an important role on the improving of UCS values of clayey soil. Also, the red mud and cement additive materials increased the freeze-thaw resistance of clayey soil against to the freeze-thaw cycles. As a result, it can be mentioned that red mud and cement additive materials can be successfully used to improve the freeze-thaw resistance of clayey soils.

### 3. REFERENCES

- [1] Aitcin, P. C., Ballivy, G., Parizeau, R., 1984. The use of condensed silica fume in grouting. Innovative Cement Grouting. Publication SP-83, ACI Detroit MI, USA, 1-18.
- [2] Arab, M.G., 2019. Soil Stabilization Using Calcium Carbonate Precipitation via Urea Hydrolysis. Proceedings of the 4th World Congress on Civil, Structural, and Environmental Engineering (CSEE'19), April, 2019, Rome, Italy.
- [3] Attom, M.F., Al-Sharif, M.M., 1998. Soil stabilization with burned olive waste. Applied Clay Science 13, 219-230.
- [4] Asavasipit, S., Nanthamontry, W., Polprasert, C., 2001. Influence of condensed silica fume on the properties of cement based solidified wastes. Cement and Concrete Research 31, 1147-1152.
- [5] Broms, B.B., Yao, L.Y.C., 1964. Shear strength of a soil after freezing and thawing. ASCE 90 (SM4), pp. 1-25.
- [6] Cetin, H., Fener, M., Gunaydin, O., 2006. Geotechnical properties of tire-cohesive clayey soil mixtures as a fill material. Engineering Geology 88 (1-2), 110-120.
- [7] Chamberlain, E.J., Iskander, I., Hunsickert, S.E., 1990. Effect of freeze-thaw cycles on the permeability and macrostructure of soils. Proc. Int. Symp. On Frozen Soil Impacts on Agricultural Range and Forest land. Special report, vol. 90-1. CRREL, Hanover, NH, USA, pp. 145-155.
- [8] Chen, F. H., 1988. Foundations on expansive soils. Elsevier.
- [9] Chu, J., Varaskin, S., Klotz, U., Mengé, P., 2009. Construction Processes, Proceedings of the 17th International Conference on Soil Mechanics and Geotechnical Engineering, 5-9 October 2009, Alexandria, Egypt, M. Hamza et al. (Eds.), IOS Press, Amsterdam, Vol. 4, pp. 3006-3135.
- [10] Eigenbrod, K.D., 1996. Effects of cyclic freezing and thawing on volume changes and permeabilities of soft fine-grained soils. Canadian Geotechnical Journal 33, 529-537.
- [11] Erguler, Z.A., Ulusay, R., 2003. A simple test and predictive models for assessing swell potential of Ankara (Turkey) Clay. Engineering Geology 67, 331-352.
- [12] Harvey, C.C., Murray, H.H., 1997. Industrial clays in the 21st century: a perspective of exploration, technology and utilization. Applied Clay Science 11, 285-310.
- [13] Indiramma, P., Sudharani, C., Needhidasan, S., 2020. Utilization of fly ash and lime to stabilize the expansive soil and to sustain pollution free environment - An experimental study. Materials Today: Proceedings 22, 694-700.
- [14] Ingles, O.G., Metcalf, J.B., 1977. Soil Stabilization Principles and Practice. 2nd ed, Australia Butterworths.
- [15] Iskander, S.M., Zhao, R., Pathak, A., Gupta, A., Pruden, A., Novak, Z.T, He, Z., 2018. A review of landfill leachate induced ultraviolet quenching substances: Sources, characteristics, and treatment. Water Research 145, 297-311.
- [16] Kalkan, E., 2003. The improvement of geotechnical properties of Oltu (Erzurum) clayey deposits for using them as barriers. Ph.D. Thesis (in Turkish), Ataturk University, Graduate School of Natural and Applied Science, Erzurum, Turkey.
- [17] Kalkan, E., 2006. Utilization of red mud as a stabilization material for the preparation of clay liners. Engineering Geology 87, 220-229.
- [18] Kalkan, E., 2009. Effects of silica fume on the geotechnical properties of fine-grained soils exposed to freeze and thaw. Cold Region Science and Technology 58, 130-135.
- [19] Kalkan, E., 2011. Impact of Impact of wetting-drying cycles on swelling behavior of clayey soils modified by silica fume. Applied Clay Science 52 (4), 345-352.
- [20] Kalkan, E., 2012. Effects of waste material-lime additive mixtures on mechanical properties of granular soils. Bulletin of Engineering Geology and the Environment 71, 99-103.
- [21] Kalkan, E., 2018. Oltu Clay Deposits (Erzurum, NE Turkey) and Their Possible Usage Areas. International Journal of Innovative Research and Reviews 2(1), 25-30.
- [22] Kalkan, E., Akbulut, S., 2004. The positive effects of silica fume on the permeability, swelling pressure and compressive strength of natural clay liners. Engineering Geology 73, 145-156.
- [23] Kalkan, E., Bayraktutan, M.S., 2008. Geotechnical evaluation of Turkish clay deposits: a case study in Northern Turkey. Environmental Geology 55, 937-950.
- [24] Kalkan, E., Yarbaşı, N., Bilici, Ö., 2019. Strength performance of stabilized clayey soils with quartzite material. International Journal of Earth Sciences Knowledge and Applications 1 (1), 1-5.
- [25] Kalkan, E., Yarbaşı, N., Bilici, Ö., 2020. The Effects of Quartzite on the Swelling Behaviors of Compacted Clayey Soils. International Journal of Earth Sciences Knowledge and Applications 2 (2), 92-101.
- [26] Kayabali, K., 1997. Engineering aspects of a novel landfill liner material: bentonite-amended natural zeolite. Engineering Geology 46 (2), 105-114.
- [27] Keith, K.S., Murray, H.H., 1994. Clay liners and barriers, In: Carr, D.D. (Ed.), Industrial Minerals and Rocks, Sixth Edition. Society for Mining, Metallurgy and Exploration, Littleton, Colorado, pp. 435-452.
- [28] Konrad, J.M., 2000. Hydraulic conductivity of kaolinite-silt mixtures subjected to closed-system freezing and

- thaw consolidation. *Canadian Geotechnical Journal* 37, 857-869.
- [29] Lambe, T.W., Whitman, R.V., 1979. *Soil Mechanics*. SI version, New York, Wiley.
- [30] Lasaki, A.G., Chenari, R.J., Sosahab, J.S., Jafarian, Y., 2018. Investigation of Strength Parameters of PVA Fiber-Reinforced Fly
- [31] Ash-Soil Mixtures in Large-Scale Direct Shear Apparatus. *Civil Engineering Journal* 4 (11), 2618-2627.
- [32] Lee, W., Bohra, N.C., Altschaeffl, A.G., White, T.D., 1995. Resilient modulus of cohesive soils and the effect of freeze-thaw. *Canadian Geotechnical Journal* 32, 559-568.
- [33] Manar, G., Hesham, B., Tareq, M., 2015. Soil Improvement Techniques. *International Journal of Scientific & Engineering Research* 6 (12), 217-222.
- [34] Murray, H.H., 2000. Traditional and new applications for kaolin, smectite, and palygorskite: a general overview. *Applied Clay Science* 17, 207-221.
- [35] Naeini, S.A., Mahdavi, A., 2009. Effect of polymer on shear strength of silty sand. *EJGE* 14, 1-11.
- [36] Naeini, S.A., Sadjadi, S.M., 2008. Effect of Waste Polymer Materials on Shear Strength of Unsaturated Clays. *EJGE* 13, 1-12.
- [37] Nelson, J.D., Miller, D.J., 1992. *Expansive Soils: Problems and Practice in Foundation and Pavement Engineering*. John Wiley and Sons, Inc., New York.
- [38] Pera, J., Boumaza, R., Ambroise, J., 1997. Development of pozzolanic pigment from red mud. *Cement and Concrete Research* 27 (10), 1513-1522.
- [39] Porebska, M., 1994. Effects of freezing on the microstructure of compacted clays. Final Report. CRREL, Hanover, USA, p. 92.
- [40] Prabakar, J., Sridhar, R.S., 2002. Effect of random inclusion of sisal fibre on strength behavior of soil. *Construction and Building Materials* 16, 123-131.
- [41] Puppala, A.J., Musenda, C., 1998. Investigation of geofiber reinforcement method on strength, swell, and shrinkage characteristic of soils. Presented at Fifth International Conference on Composites Engineering, Las Vegas.
- [42] Sabtan, A.A., 2005. Geotechnical properties of expansive clay shale in Tabuk, Saudi Arabia. *Journal of Asian Earth Science* 25, 747-757.
- [43] Sandra, T., Jeffrey, C.E., 1992. The effects of filler and admixtures on grout performance. *Grouting, Soil Improvement, and Geosynthetics*. Geotechnical Engineering Division of ASCE, USA 1, 337-349.
- [44] Simonsen, E., Isacsson, U., 2001. Soil behavior during freezing and thawing using variable and constant confining pressure triaxial tests. *Canadian Geotechnical Journal* 38, 863-875.
- [45] Simonsen, E., Janoo, V.C., Isacsson, U., 2002. Resilient properties of unbound road materials during seasonal frost conditions. *Journal of Cold Regions Engineering ASCE* 16, 28-50.
- [46] Viklander, P., Eigenbrod, D., 2000. Stone movements and permeability changes in till caused by freezing and thawing. *Cold Regions Science and Technology* 31, 151-162.
- [47] Yang, M., Yao, T., Gou, X., Koike, T., He, Y., 2003. The soil moisture distribution, thawing-freezing processes and their effects on the seasonal transition on the Qinghai-Xizang (Tibetan) plateau. *Journal of Asian Earth Sciences* 21, 457-465.
- [48] Yarbaşı, N., Kalkan E., 2019. The Stabilization of Sandy Soils by Using the Plastic Bottle Waste. *International Journal of Advance Engineering and Research Development* 6 (11), 140-144.
- [49] Yarbaşı, N., Kalkan E., 2020. The Mechanical Performance of Clayey Soils Reinforced with Waste PET Fibers. *International Journal of Earth Sciences Knowledge and Applications*, 2(1) 19-26.
- [50] Yarbaşı, N., Kalkan, E., 2021. Freeze-Thaw Resistance of Fine-Grained Soils Stabilized with Waste Material Mixtures. *International Journal of Science and Engineering Applications* 9 (12), 158-163.
- [51] Yong, R.N., Boonsinsuk, P., Yin, C.W.P., 1985. Alteration of soil behavior after cyclic freezing and thawing. *Proc. 4th Int. Symp. Ground Freezing, Sapporo*, pp. 187-195.
- [52] Zhang, S., Lai, Y., Zhang, X., Pu, Y., Yu, W., 2004. Study on the damage propagation of surrounding rock from a cold-region tunnel under freeze-thaw cycle condition. *Tunnelling and Underground Space Technology* 19 (3), 295-302.

# Effects of Quartzite on the Desiccation Cracks of Clayey Soils Exposed to Wetting-Drying Cycles

Necmi Yarbaş  
Department of Civil Engineering  
Engineering Faculty  
Ataturk University  
Erzurum, Turkey

Ekrem Kalkan  
Department of Civil Engineering  
Engineering Faculty  
Ataturk University  
Erzurum, Turkey

**Abstract:** The compacted clayey soils crack on drying because of their high swelling potential, and their hydraulic conductivities increase. To solve this problem, it is essential to stabilize the clayey soils using additive materials. The aim of this study is to examine the suitability of quartzite as a stabilization material to reduce the development of desiccation cracks in compacted clayey liner and cover systems. Experimental study was conducted to investigate the effect of wetting-drying cycles on the initiation and evolution of cracks in compacted clayey soils. For experimental studies, seven samples were prepared stabilized by using 0%, 2.5%, 5%, 7.5%, 10%, 12.5% and 15% quartzite and then they were subjected to four subsequent wetting-drying cycles. The results show that quartzite decreases the development of desiccation cracks on the surface of compacted samples. It is concluded that quartzite as a geological material can be successfully used to reduce the development of desiccation cracks in compacted clayey liner and cover systems exposed wetting-drying cycles.

**Keywords:** Clayey soil, quartzite, soil stabilization, desiccation cracks, wetting-drying cycles

## 1. INTRODUCTION

The clayey soils generally classified as expansive soils tend to expand as they absorb water and will shrink as water is drawn away. They contain clay minerals that have the potential for swelling and shrinkage under changing moisture contents. Clay minerals could originate from the weathering of shale, slate, sandstone, and limestone. Another source is the diversification of volcanic ash deposited under marine conditions during geologic times, settled alone or mixed with shale or limestone (Grim 1968; Kalkan and Bayraktutan, 2008).

Expansive soils are known to cause severe damage to structures resting on them. However, these soils are very important in geology, construction, and for environmental applications, due to their wide usage as impermeable and containment barriers in landfill areas and other environmentally related applications (Erguler and Ulusay, 2003; Harvey and Murray, 1997; Kayabali, 1997; Keith and Murray 1994; Murray, 2000; Sabtan, 2005). Safe and economic designs of foundations on clayey soils and performance of compacted clayey soils for geotechnical purposes require the knowledge of swelling characteristics such as swelling pressure, swelling potential and swelling index. Cyclic drying and wetting phenomena can cause progressive deformation of expansive clayey soils, which may affect building foundations, drainage channels, buffers in radioactive waste disposals, etc. (Guney et al., 2007; Nowamooz and Masrouri, 2008; Rao et al., 2001; Kalkan, 2011; Kalkan et al., 2020).

The formation of desiccation cracks on soil surface due to loss of water is a common phenomenon in nature. This behavior significantly affects the performance of soil in various geotechnical, geological and environmental applications. Generally, the presence of cracks in soil would increase the compressible and reduce the overall mechanical strength (Morris et al., 1992). The hydraulic properties of soil are directly influenced by crack networks in soil (Chertkov, 2000). There are numerous laboratory experiments conducted

to investigate the initiation and propagation of desiccation crack in soils (Miller et al., 1998; Nahlawi and Kodikara, 2006; Tang et al., 2008; Tang et al., 2011; Tang et al., 2016; Kalkan, 2020; Yarbaşı and Kalkan, 2020).

The main requirements of liners are the minimization of pollutant migration, low swelling and shrinkage and resistance to shearing (Brandl, 1992; Kayabali, 1997; Cazaux and Didier, 2000). Some recent applications include those for environmental purpose, such as impermeable layers in landfills, which act as horizontal or vertical contaminant barriers. The close proximity of compacted clayey soil systems to the atmosphere leaves a compacted clayey layer unprotected, and prone to damage from desiccation. Compacted clayey layers in earthen covers undergo seasonal changes in water content, even at significant depths, due to seasonal variations in precipitation and evapotranspiration (Daniel and Wu, 1993; Sharma and Levis, 1994; Khire et al., 1997; Albrecht and Benson, 2001; Mal et al., 2008).

The swelling potential of expansive soils can be controlled by different methods including soil improvement by chemical additives, treatment by electroosmosis application, compaction control, moisture control, rewetting, and thermal methods (Kalkan, 2011; Goodarzi et al. 2016; Kalkan et al., 2019; Kherad et al. 2020). The application of both the traditional and non-traditional additives in treatment of expansive soils has been widely studied by various researchers from different parts of the world (Pooni et al. 2019; Goodarzi et al. 2015; Seco et al. 2011). Lime, cement, and gypsum are considered as traditional additives and are known as appropriate additives for reducing the swelling potential and increasing the strength of soils (Shahsavani et al., 2020). In the chemical stabilization, some additives such as lime, cement, fly ash, silica fume etc., are added, which physically interacts with the soil and change the index properties (Chen, 1988; Çokça, 2001; Kalkan and Akbulut, 2004; Kalkan, 2009; Kalkan, 2011; Jamsawang et al., 2017; Chittoori et al., 2018; Kalkan et al., 2019).

The basic objective of this research is to investigate the effects of quartzite on the desiccation cracks of clayey soils exposed to wetting-drying cycles. For this purpose, clayey soil was stabilized by using quartzite as geological material at different content.

## 2. MATERIAL and METHODS

### 2.1. Clayey Soil

The clayey soil was supplied from the clay deposits of Oltu Oligocene sedimentary basin, Erzurum, NE Turkey. This soil was placed in plastic bags and transported to a soil mechanics laboratory. This clayey soil is over-consolidated and it has clayey-rock characteristics in natural conditions. It is defined as a high plasticity soil according to the Unified Soil Classification System (Kalkan, 2003; Kalkan and Bayraktutan, 2008). Its granulometry curve was given in Figure 1.

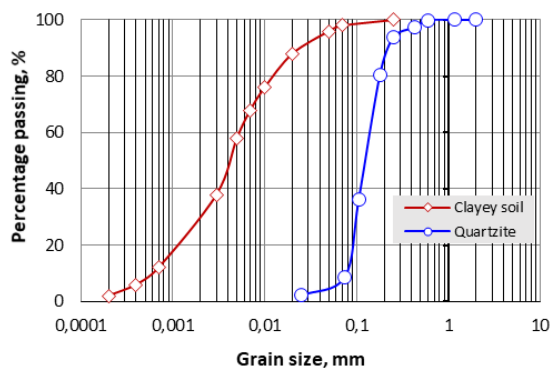


Figure 1. Grain size distribution of clayey soil, red mud and cement

### 2.2. Quartzite

In this experimental study, the quartzite was used as additive material. It was supplied from Demirözü district of Bayburt, NE Turkey. It is a metamorphic rock formed by compaction and recrystallization of quartz sandstone. This quartzite, which has an ortho-quartzite formation, contains feldspar, mica, clay, magnetite, hematite, garnet rutile and limestone. There is more than 95% quartz in its composition (Kalkan et al., 2019). Its granulometry curve was given in Figure 1.

### 2.3. Experimental Procedure

The clayey soil and quartzite-clayey soil mixtures were compacted at the optimum moisture content in cylindrical mold with 50 mm diameter and 30 mm height. The compacted samples were subjected to four drying-wetting cycles under room temperature ( $20 \pm 2$  °C). After 7 days drying period, the samples were saturated with water. After saturation, the samples were exposed a new drying process. They were dried for 7 days. Each end of wetting-drying cycles, the samples were imaged.

## 3. Results and Discussion

To investigate the effects of quartzite on the desiccation cracks, the compacted clayey soil samples and quartzite stabilized-clayey soil samples were exposed to wetting-drying cycles. The observations showed that the quartzite improved the clayey soil. At the end of first drying cycle, the cracking effect decreased in stabilized clayey soil samples with increasing quartzite contents. In the stabilized clayey soil

samples with 10%, 12,5% and 15% quartzite content, no cracks developed (Figures 2-5).

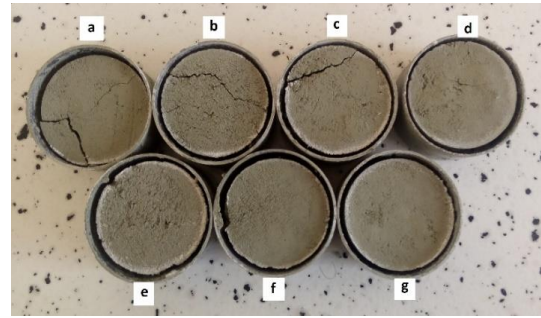


Figure 2. Typical crack patterns captured at first drying process (a: 0%, b: 2.5%, c: 5%, d: 7.5%, e: 10%, f: 12,5% and g: 15% quartzite)

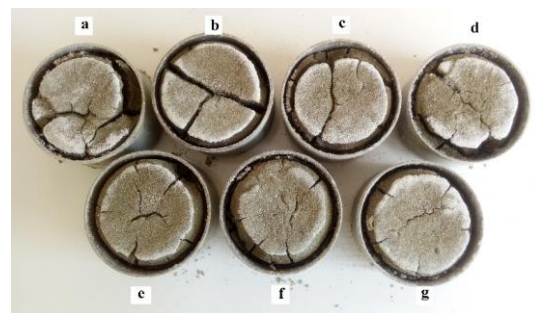


Figure 3. Typical crack patterns captured at second drying process (a: 0%, b: 2.5%, c: 5%, d: 7.5%, e: 10%, f: 12,5% and g: 15% quartzite)

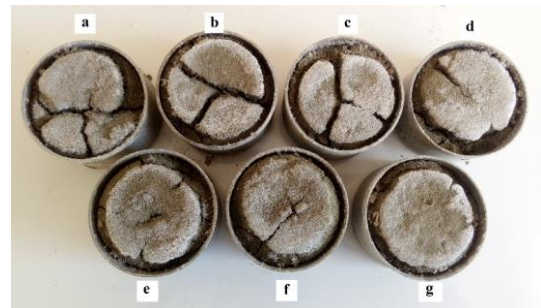


Figure 4. Typical crack patterns captured at third drying process (a: 0%, b: 2.5%, c: 5%, d: 7.5%, e: 10%, f: 12,5% and g: 15% quartzite)

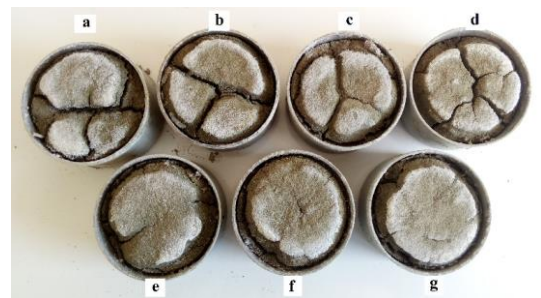


Figure 5. Typical crack patterns captured at fourth drying process (a: 0%, b: 2.5%, c: 5%, d: 7.5%, e: 10%, f: 12,5% and g: 15% quartzite)

In the stabilized clayey soil samples with 10%, 12,5% and 15% quartzite content, very small cracks occurred or no cracks developed. The improve in the resistance of clayey soil samples against to desiccation crack development under wetting-drying cycles was attributed to the addition of low-plastic material to the clayey soil material (Attom and Al-Sharif, 1998; Di Maio et al., 2004; Kalkan and Akbulut, 2004; Kalkan, 2009; Kalkan et al., 2020).

In Figures 2-5, it is interesting to found that the cracks initiated at the boundaries are almost perpendicular to the tangent direction, pointing to the centre of the soil sample. This is attributed to the boundary effect. The soil shrinkage during the drying process results in a separation away from the vertical walls of the mold and creates cracks along the boundary direction (Tang et al., 2011, Cui et al., 2014; Cheng et al., 2021).

### 3. CONCLUSIONS

In this study, the effect of quartzite geological material on the desiccation crack behaviors for clayey soils exposed to the wetting-drying cycles. It was seen that quartzite decreased the development of desiccation cracks on the surface of clayey soil-quartzite mixture samples under wetting-drying cycles. As a result, it can be stated that quartzite as a natural material can be used to minimize the development of desiccation cracks under wetting-drying cycles. Also, it can potentially reduce stabilization costs by utilizing wastes in a cost-effective manner.

### 3. REFERENCES

- [1] Attom, M.F., Al-Sharif, M.M., 1998. Soil stabilization with burned olive waste. *Applied Clay Science* 13, 219-230.
- [2] Bell, F.G., 1993. *Engineering treatment of soils*, Published by E and FN Spon, an imprint of Chapman and Hall, Boundary Row, London.
- [3] Chen, F.H., 1988. *Foundations on Expansive Soils*. Elsevier Scientific Publishing, Amsterdam.
- [4] Cheng, Q., Tang, C-S., Xu, D., Zeng, H., Shi, B., 2021. Water infiltration in a cracked soil considering effect of drying-wetting cycles. *Journal of Hydrology* 593, 125640.
- [5] Chertkov, V.Y., 2000. Using Surface Crack Spacing to Predict Crack Network Geometry in Swelling Soils. *Soil Science Society of America Journal* 64 (6), 1918-1921.
- [6] Chittoori, B.C., Mishra, D., Islam, K.M., 2018. Forensic investigations into recurrent pavement heave from underlying expansive soil deposits. *Transportation Research Record Journal of the Transportation Research Board*, 0361198118758625.
- [7] Cokca, E., 2001. Use of class C fly ashes for the stabilization of an expansive soil. *Journal of Geotechnical and Geoenvironmental Engineering* 127 (7), 568-573.
- [8] Cui, Y.J., Tang, C.S., Tang, A.M., Ta, A.N., 2014. Investigation of soil desiccation cracking using an environmental chamber
- [9] *Rivista Italiana di Geotecnica*, 24 (1), 9-20.
- [10] Di Maio, C., Santoli, L., Schiavone, P., 2004. Volume change behaviour of clays: the influence of mineral composition, pore fluid composition and stress state. *Mechanics of Materials* 36, 435-451.
- [11] Erguler, Z.A., Ulusay, R., 2003. A simple test and predictive models for assessing swell potential of Ankara (Turkey) Clay. *Engineering Geology* 67, 331-352.
- [12] Goodarzi, A.R., Akbari, H.R., Salimi, M., 2016. Enhanced stabilization of highly expansive clay by mixing cement and silica fume. *Applied Clay Science* 132-133, 675-684.
- [13] Grim, R.E., 1968. *Clay Mineralogy*. McGraw Hill, New York. p 596.
- [14] Guney, Y., Sari, D., Cetin, M., Tuncan, M., 2007. Impact of cyclic wetting-drying on swelling behavior of lime-stabilized soil. *Building and Environment* 42, 681-688.
- [15] Harvey, C.C., Murray, H.H., 1997. Industrial clays in the 21st century: a perspective of exploration, technology and utilization. *Applied Clay Science* 11, 285-310.
- [16] Jamsawang, P., Nuansrithong, N., Voottipruex, P., Songpiriyakij, S., Jongpradist, P., 2017. Laboratory investigations on the swelling behavior of composite expansive clays stabilized with shallow and deep clay-cement mixing methods. *Applied Clay Sciences* 148, 83-94.
- [17] Kalkan, E., 2009. Effects of silica fume on the geotechnical properties of fine-grained soils exposed to freeze and thaw. *Cold Region Science and Technology* 58, 130-135.
- [18] Kalkan, E., 2011. Impact of wetting-drying cycles on swelling behavior of clayey soils modified by silica fume. *Applied Clay Science* 52 (4), 345-352.
- [19] Kalkan, E., 2012. Effects of waste material-lime additive mixtures on mechanical properties of granular soils. *Bulletin of Engineering Geology and the Environment* 71 (1), 99-103.
- [20] Kalkan, E., 2020. A Review on the Microbial Induced Carbonate Precipitation (MICP) for Soil Stabilization. *International Journal of Earth Sciences Knowledge and Applications* 2(1), 38-47.
- [21] Kalkan, E., Akbulut, S., 2004. The positive effects of silica fume on the permeability, swelling pressure and compressive strength of natural clay liners. *Engineering Geology* 73, 145-156.
- [22] Kalkan, E., Bayraktutan, M.S., 2008. Geotechnical evaluation of Turkish clay deposits: a case study in Northern Turkey. *Environmental Geology* 55, 937-950.
- [23] Kalkan, E., Yarbaşı, N., Bilici, Ö., 2019. Strength performance of stabilized clayey soils with quartzite material. *International Journal of Earth Sciences Knowledge and Applications* 1 (1), 1-5.
- [24] Kalkan, E., Yarbaşı, N., Bilici, Ö., 2020. The Effects of Quartzite on the Swelling Behaviors of Compacted Clayey Soils. *International Journal of Earth Sciences Knowledge and Applications* 2 (2), 92-101.
- [25] Kayabali, K., 1997. Engineering aspects of a novel landfill liner material: bentonite-amended natural zeolite. *Engineering Geology* 46, 105-114.
- [26] Keith, K.S., Murray, H.H., 1994. Clay liners and barriers, In: Carr, D.D. (Ed.), *Industrial Minerals and Rocks*, Sixth Edition. Society for Mining, Metallurgy and Exploration, Littleton, Colorado, pp. 435-452.
- [27] Kherad, M.K., Vakili, A.H., bin Selamat, M.R., Salimi, M., Farhadi, M.S., Dezh, M., 2020. An experimental

- evaluation of electroosmosis treatment effect on the mechanical and chemical behavior of expansive soils. *Arabian Journal of Geosciences* 13 (6), 1-12.
- [28] Morris, P.H., Graham, J., David, J., 1992. Cracking in drying soils. *Canadian Geotechnical Journal* 4 (1), 263-277.
- [29] Miller, C.J., Mi, H., Yesiller, N., 1998. Experimental Analysis of Desiccation Crack Propagation in Clay Liners. *Journal of the American Water Resources Association* 43 (3), 677-686.
- [30] Murray, H.H., 2000. Traditional and new applications for kaolin, smectite, and palygorskite: a general overview. *Applied Clay Science* 17, 207-221.
- [31] Nahlawi, H., Kodikara, J.K., 2006. Laboratory experiments on desiccation cracking of thin soil layers. *Geotechnical and Geological Engineering* 24, 1641-1664.
- [32] Nowamooz, H., Masroufi, F., 2008. Hydromechanical behaviour of an expansive bentonite-silt mixture in cyclic suction-controlled drying and wetting tests. *Engineering Geology* 101, 154-164.
- [33] Okagbue, C.O., Onyeobi, T.U.S., 1999. Potential of marble dust to stabilize red tropical soils for road construction. *Engineering Geology* 53, 371-380.
- [34] Pooni, J., Giustozzi, F., Robert, D., Setunge, S., O'Donnell, B., 2019. Durability of enzyme stabilized expansive soil in road pavements subjected to moisture degradation. *Transportation Geotechnics* 21, 100255.
- [35] Rao, S.M., Reddy, B.V.V., Muttharam, M., 2001. The impact of cyclic wetting and drying on the swelling behavior of stabilized expansive soils. *Engineering Geology* 60, 223-233.
- [36] Sabtan, A.A., 2005. Geotechnical properties of expansive clay shale in Tabuk, Saudi Arabia. *Journal of Asian Earth Science* 25, 747-757.
- [37] Schmitz, R.M., Schreoder, C., Charlier, R., 2004. Chemo-mechanical interactions in clay: a correlation between clay mineralogy and Atterberg limits. *Applied Clay Science* 26, 351-358.
- [38] Seco, A., Ramirez, F., Miqueleiz, L., Garcia, B., 2011. Stabilization of expansive soils for use in construction. *Applied Clay Science* 51, 348-352.
- [39] Shahsavani, S., Vakili, A.H., Mokhberi, M., 2020. The effect of wetting and drying cycles on the swelling-shrinkage behavior of the expansive soils improved by nanosilica and industrial waste. *Bulletin of Engineering Geology and the Environment* 79, 4765-4781.
- [40] Sivapullaiah, P.V., Sridharan, A., Bhaskar, R.K.V., 2000. Role of amount and type of clay in the lime stabilization of soils. *Ground Improvement* 4, 37-45.
- [41] Tang, C.S., Cui, Y.J., Shi, B., Tang, A.M., An, N., 2016. Effect of wetting-drying cycles on soil desiccation cracking behaviour. *E3S Web of Conferences* 9, 12003 (E- 2016).
- [42] Tang, C.S., Shi, B., Liu, C., Gao, L., Inyang, H.I., 2011. Experimental investigation of the desiccation cracking behavior of soil layers during drying. *Journal of Materials in Civil Engineering* 23 (6), 873-878.
- [43] Tang, C.S., Shi, B., Liu, C., Zhao, L., Wang, B., 2008. Influencing factors of geometrical structure of surface shrinkage cracks in clayey soils. *Engineering Geology* 101, 204-217.
- [44] Yarbaşı, N., Kalkan, E., 2020. The Mechanical Performance of Clayey Soils Reinforced with Waste PET Fibers. *International Journal of Earth Sciences Knowledge and Applications* 2 (1), 19-26.

# Geospatial Technologies in Waste Management: A Case Study of Rivers State Waste Management Agency (RIWAMA)

Robinson Tombari Sibe  
Rivers State University,  
Port Harcourt  
Rivers State, Nigeria

Ian Abraham Gobo  
Rivers State Waste Management Agency,  
Port Harcourt,  
Rivers State, Nigeria

---

**Abstract:** Waste Management can be quite challenging, especially in the developing world. The challenge becomes even more complex with the growing population. City planners and decision makers are turning to technology to improve the efficiency of the waste management process. Geospatial technologies have offered a range of solutions, which have been deployed with success in waste management. This paper highlights the challenges of waste management in Port Harcourt, Nigeria, and how the Rivers State Waste Management Agency (RIWAMA) deployed the use of GIS in solving most of the challenges of identification, planning, evacuation, and transportation of wastes within the Port Harcourt metropolis. This paper looked at how this solution was deployed to solve key challenges as well as stimulate citizen participation in the waste management process. The paper concludes with a set of recommendations for expanding the potentials of its application.

**Keywords:** Web GIS; Mobile GIS; Waste Management; Waste Management Application; GIS; Geospatial Application; RIWAMA; RIWAMA Geospatial Application; Open-Source GIS.

---

## 1. INTRODUCTION

The City of Port Harcourt is one of the most populous cities in Nigeria. As the hub of the hydrocarbon industry in Nigeria, the city has witnessed exponential growth in population in the last few decades. From a 1991 census figure of 440,399 the city grew to 1,005,904 in 2006, (Nna & Pabon, 2012). The colonial city founded a little over a hundred years ago has also witnessed exponential expansion in size, reflective of the demographic push. From a size of 15.54 sq.km in 1914 when Nigeria was amalgamated, the city expanded to an area of 360 sq.km by the 1980's (Wizor, 2014). With this exponential growth in population, comes the challenge of waste management. This is one of the key challenges of urbanization (Elenwo, 2015), and Port Harcourt has had her fair share of the challenge. City planners continue to turn to technology to solve this problem, and this paper will x-ray one of such solutions – Geographic Information System (GIS).

## 2. GEOSPATIAL TECHNOLOGIES

Geospatial technologies are tools used for acquiring, processing, manipulating, analyzing, and storing georeferenced data. These technologies have evolved over the years, with evolving technologies. Examples today, includes Geographic Information System (GIS), GPS, Remote Sensing, etc. For this paper, we shall zero in more on GIS. There is no single detailed and articulated history of what is known as GIS, because it evolved through multiple parallel, but separate applications across numerous disciplines (Pickles, 1999). Although there are multiple claims as to the exact origin, however, what is today known as GIS began about 1960, following the discovery that maps could be programmed using simple code and then stored in a computer allowing for future modification when necessary. GIS has evolved with the technologies through the years. From being deployed in mainframe computers, it evolved through the desktop GIS, to Web and Mobile Platforms (Sibe, 2009). The use of the Web

as a dissemination medium for maps can be regarded as a major advancement in cartography and opened many new opportunities, such as real time maps, cheaper dissemination, more frequent and cheaper updates of data and software, personalized map content, distributed data sources and sharing of geographic information (Neumann, 2007). Today, interactive maps are served seamlessly through mobile phones.

The National Center of Geographic Information and Analysis (NCGIA) defines GIS as a system of hardware, software, and procedures to facilitate the management, manipulation, analysis, modeling, representation and display of georeferenced data to solve complex problems regarding planning and management of resource. It is a simplified, yet systematic way of representing geographic reality in a digital platform. Geospatial technologies have evolved from the static computer mapping of the 70's to Spatial Database Management in the 80's, Map Analysis/Modeling in the 90's and the web-based spatial solutions of today, allowing millions of ordinary users to take advantage of the technology to solve complex challenges (Ghosh et al, 2012). The proliferation of web-based solutions has opened a new vista of opportunity to a wide range of application areas and a seemingly unending audience. Governments across the world are leveraging these to offer smart governance (Sibe, 2014).

A GIS can perform complicated analytical functions and then present the results visually as maps, tables or graphs, allowing decision-makers to virtually see the issues before them and then select the best course of action. The advent of GIS has broadened the application areas of mapping. GIS has changed from been just a tool for mapping physical geographic features to a tool that can map just about any feature – from physical to socioeconomic, as long as it can be tied to some geography. Another great feature of mapping applications is that it allows for different layers of information to be combined, analysed and studied in relation to each other. With

GIS, trends could be revealed, patterns extracted and scenarios simulated (Sibe, 2010).

### 3. GIS AND WASTE MANAGEMENT

As cities grow, their waste challenges become more challenging. Thus, city Planners have continued to turn to technology, to improve their effectiveness. GIS is one of such technologies that have proved quite effective. GIS offers planners the ability to visualize the solid waste situations and facilitate route analysis through mapping (Shoba & Rasappan, 2013). Waste data has a spatial component, therefore, GIS remains an important tool in planning and management.

Studies have shown that in developing countries, the major causes of solid waste management problems can be traced to poor linkages between spatial and non-spatial data components of the waste management process. The issues, such as inefficient waste collection, high operational costs, uncoordinated collection point, etc., can all be traced to the poor linkages (Kyessi & Mwakalinga, 2009). GIS serves as the perfect solution to bridge these linkages. GIS has been deployed by decision makers in modeling, analyzing, and simulating various challenges relating to Solid Waste Management. It has been deployed successfully, for performing tasks such as, siting of communal receptacles, transfer stations and landfills, optimizing the collection and transportation, and local forecasting of waste. These spatial modeling tools have been key to collection and transport optimization, as well as boost overall efficiency of the entire waste management process (Kallel, et al., 2016).

### 4. THE WASTE MANAGEMENT CHALLENGE IN PORT HARCOURT

The city of Port Harcourt has been contending with the challenges of management over the years. Solid Waste can be sighted along the major roads, with heaps of dumps lining some streets (Agwu, 2012). A drive through the city will reveal the heaps of solid waste lined up the roads especially at the approved dumping times of RIWAMA. Even the median strips are not spared, as residents have converted the medians as refuse receptacle points. Some of the reasons for this reckless dumping, include, insufficient litter bins and receptacles, poor awareness by the citizens, citizens indiscipline and irresponsibility, and inadequate refuse collection services. As a result of the littering many drains are blocked with water pollution becoming an imminent public health issue (Tamunobereton-ari et al., 2012).

In Rivers State, the Agency saddled with the responsibility of Waste Management is the Rivers State Waste Management Agency (RIWAMA). They have the responsibility of collecting wastes from receptacles and disposing same in designated dump sites. It was a creation of an Act of the Rivers State House of Assembly in 2017 and given the statutory responsibility of maintaining a clean environment (Obuah & Okon, 2017). Currently, residents are expected to bag their wastes and drop them at designated receptacles, for onward pick up by RIWAMA Waste Contractors. Due to a myriad of challenges, this method has proved visibly inefficient and unsustainable.

Some of the challenges we observed before the take-off of the project, includes:

- (1) Shortage of Waste Contractors
- (2) Receptacles are not mapped or clearly marked. Thus, residents in most cases claim not to know the nearest receptacle. In most cases, receptacles were created "spontaneously" by citizens. Citizens clearly did not know the approved receptacles, as sustained

illegal dumping of waste at a particular point, tends to "legitimize" the use as a receptacle over time.

- (3) Zones were not mapped out based on volumes of wastes generated; they were identified based on convenience of collection. That is, there was no articulated map that clearly delineates the city to zones, for ease of planning and management.
- (4) Citizens were detached from the waste management process. No framework for citizens engagement. No clear channels of communication.
- (5) Since the Agency did not use technology, enforcement was through a Task Force approach; a method that is both inefficient and expensive.
- (6) Lack of effective supervision and performance tracking of contractors.
- (7) Citizens dumping outside of the prescribed timetable. Thus, in some case, they dump after the Waste Contractor had evacuated waste from the receptacle for that day.
- (8) Operations, planning, and management was not scientific and precise.
- (9) Mode of refuse collection has remained cumbersome with workers manually loading refuse trucks rather than automated equipment.
- (10) No tools for analytics, quite critical for strategic and contingency planning.

To address these challenges, RIWAMA commissioned E-Sense Technologies Ltd, an indigenous geospatial technology company, to develop a geospatial application to achieve the following:

- (1) Geolocation of all Receptacles and Dumpsites
- (2) Design a Portal that integrates the website and the mapping component. The geospatial portal should facilitate planning and management of the process.
- (3) A Mobile App to stimulate citizen participation.
- (4) Social Media Integration

## 5. METHODOLOGY

### 5.1 User Needs Assessment and System Analysis

The first task was to go through the processes with the staff of RIWAMA, to understand how things were done manually. Designated staff were interviewed to understand the current manual process. Contractors were also interviewed to understand things from their perspective. Also, citizens were randomly sampled to share their perspectives on the current challenges associated with the current system of waste management. Our design was shaped by our findings from this interaction.

### 5.2 Field Data Collection

Our Field staff visited the various receptacles and dump sites in the areas of coverage, consisting of Port Harcourt City LGA, Obio Akpor LGA, Oyigbo LGA and Eleme LGA. At each receptacle, our team, armed with a field notepad, a GPS and a Digital Camera, took pictures and GPS coordinates. They also noted the landmarks as well as nearest known address.

### 5.3 Quality Control

Data gotten from the field went through series of quality control to ensure integrity, precision, and spatial sense. The field data officer submitted data entered to a quality control officer to evaluate for accuracy, precision, and integrity. Once

data passes our quality control tests, they were harmonized and saved in the geospatial database.

### 5.4 Mapping and Geospatial Analysis

Maps were produced showing all the receptacles and dumpsites. Also, routes were mapped. Before this time, the road lengths were not accurately established; we achieved this easily, using GIS. This is quite important as the designated dumpsites were hitherto randomly chosen, without any scientific basis. Also, the zones were mapped out, for ease of administration. This was necessary for effective planning. The visualization capacity of GIS made this quite easy and interesting. ESRI ArcMap Software was used for the mapping process.

### 5.5 Web Application Analysis

At the time of this project, the Agency did not even have a functional website. Therefore, we had to create one that integrated the spatial components. Thus, once you got to the website, you could perform very complex geospatial analysis, without having sophisticated GIS knowledge. One of the key advantages of serving GIS on the web is that it allows people with less GIS sophistication, to perform complex GIS analysis and functions. To reduce cost, the application was deployed using opensource platform. Also, to drive down cost of data acquisition, we leveraged existing data, by building the application on the Google platform. This gave us access to quality datasets at almost no cost. By building on the Google platform, we also leveraged their huge popularity, to serve the application to more persons.

### 5.6 Mobile Application Design

#### Mobile Application Design

Nigeria has about 191 million active mobile lines (Nigerian Communications Commission, 2021). More and more Nigerians are surfing the web with their mobile phones. Thus, we had to leverage this impressive mobile tele-density to stimulate citizen participation in Waste Management. Thus, we designed a mobile application, using the most modern programming toolset on the Open-Source Platform. The Mobile Application was deployed on Android Playstore, so that members of the public can download for free.

## 6. RESULTS

Figures 1-5 shows some of the key functionalities of the RIWAMA geospatial application. The Web Application has the following functionalities:

- (1) An admin module that allows you manage the portal. Using this function, the administrator can manage users and processes, post news items in real time, approve posts and respond to citizen-posts.
- (2) Users can perform complex administrative and spatial analysis, without having sophisticated GIS functions.
- (3) Upload spatial coordinates, pictures and other key attributes of receptacles and dumpsites.
- (4) Search for nearest receptacle. This search will automatically spool out the results of the three closest waste facilities.
- (5) Report any incidence, such as defaulting contractors or illegal receptacle. Citizens can quickly and easily

report such incidences with detail, from their mobile phones. Such reports automatically pick the coordinates of the citizen, or allow user input the address manually. Pictures can also be attached to reports; this makes it quite graphic and accurate. When using a desktop or laptop, the application relies on the location component of your service provider.

- (6) Administrator can register Contractors and Service Providers.
- (7) View news feeds
- (8) Perform complex analysis, such as tonnage analysis. This automatically computes the tones per zone, and outputs a graph. Please note that this will be done based on the information supplied.
- (9) Functionality to toggle between the map view and the satellite imagery view.

Figures 6 and 7 shows screen shots of the RIWAMA Geospatial Mobile Application. The Mobile Application has the following key functionalities:

- (1) View Maps – This defaults to your current location.
- (2) Query Nearest Waste Facilities – This will spool the three nearest waste point on an interactive map.
- (3) Query Facilities based on specified address.
- (4) Report Incidences – Citizens can report incidences in real time. For example, citizens can report illegal dump sites or defaulting contractors.
- (5) Sign-up/Sign-in as a vendor



Figure 1. RIWAMA Web Portal with Geospatial Component

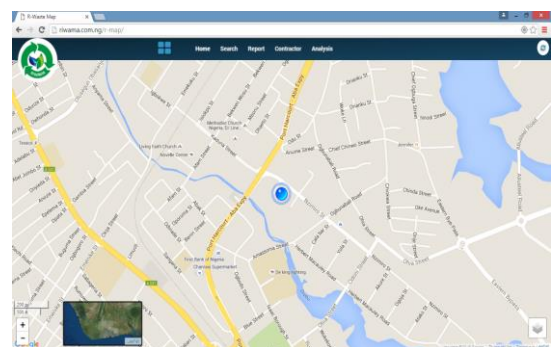


Figure 2. Web Component of Mapping Application

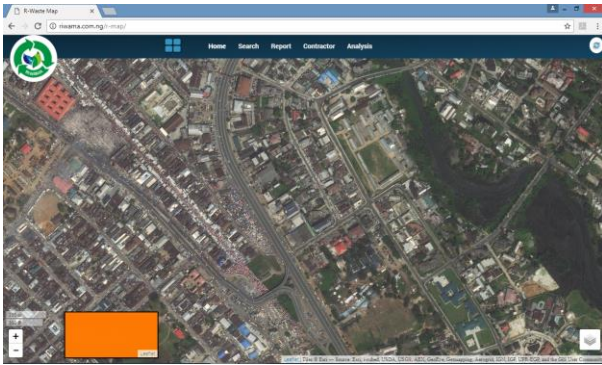


Figure 3. Web Mapping Application showing Satellite Imagery View

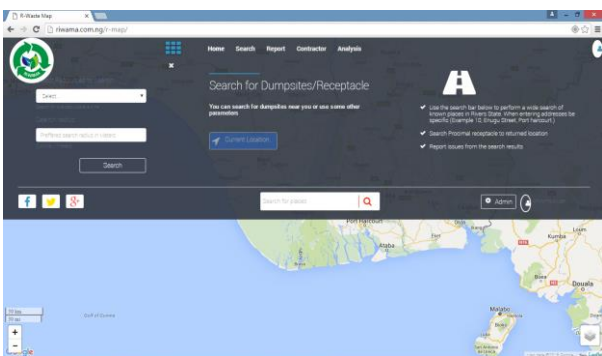


Figure 4. Web Mapping Application showing Search Tool

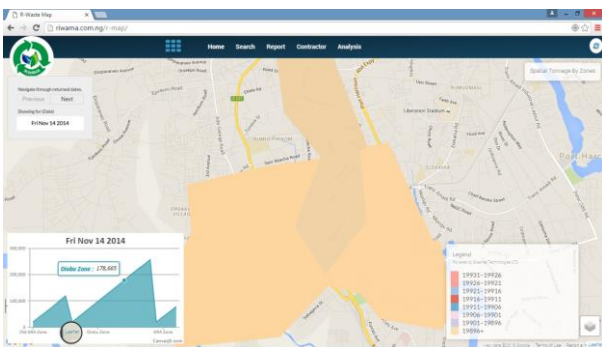


Figure 5. Web Mapping Application showing Solid Waste Tonnage Analysis

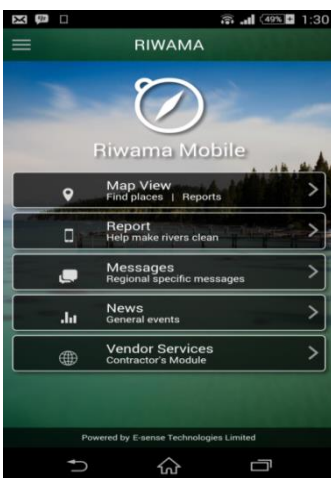


Figure 6. Home Screen of the RIWAMA Mobile Application

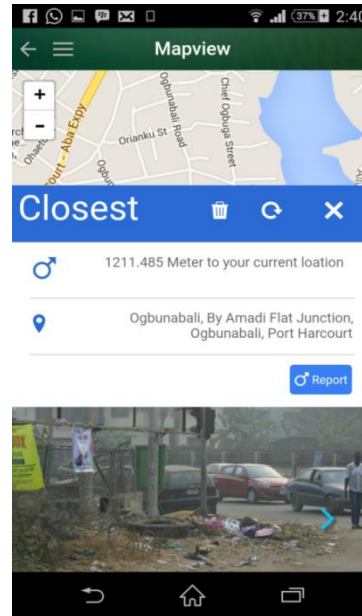


Figure 7. Search Result for Nearest Dumpsite

## 7. CONCLUSION AND RECOMMENDATIONS

The project was a huge success, especially considering the funding limitations. The application has automated most of the key back-end functions, bring precision in the planning process. One of the key challenges solved was the stimulation of citizen-participation in the waste management process. This solution allowed citizen to report incidences and defaulting contractors.

An ordinary user, with a working knowledge of Web browsers, or with an Android phone, could perform tasks hitherto restricted to the GIS user with sophisticated skills. This ensured that more and more users become “spatially aware” and location sensitive. Governments across the globe and especially in developing countries can leverage the potentials of low-cost Web-based GIS applications like this for planning and effective governance.

Below are some recommendations:

1. In Rivers State, Waste Management is still seen as a government service. That is clearly not sustainable. Waste Management is big business. To professionalize this sector, there should be more private sector participation. Government may continue to regulate, but the core of the services should be private sector driven. This will bring in more professionalism, and more investment to the sector.
2. Residents should be made to pay for waste management services as a part of utility services being rendered by the agency and the contractors. This will reduce or eliminate the overbearing control of government on the sector that should be largely private sector driven.
3. The current application focused more on stimulating citizen-participation. There’s a proposed module to handle more tracking related functions for the Agency and Waste Contractors. This module would be key to performance monitoring and supervision, and it is highly recommended.
4. It is one thing to develop an application; it’s another thing to maximize the application. The agency

needs to do more to maximize usage and stimulate participation from citizens.

5. There is the human component in every system. Technology itself needs the human input. Where this is lacking, success will be dwarfed. For this to be a success, citizens would like to see responsiveness. For example, if citizens see timely response to their reports, they'll have more faith in the application.
6. There are other possible channels this can be deployed (Apple Store, Blackberry Store, etc). The application needs to be deployed on these other channels to serve more citizens.
7. Data is key to any successful GIS project. The accuracy and efficiency of the GIS application is hinged on the quality of the datasets. It is important that data should be updated more often than is currently done.
8. Waste Management is not just about collection and transportation. It goes beyond that to sorting, treatment, recycling, etc. This application only facilitates collection and decision support; the rest of the tasks will depend on the Agency's investment in other forms of technology, that will handle these.
9. Data Gathering was limited to 4 LGAs. We recommend that this be extended to cover the entire Rivers State.
10. People only get to use an app that they know exist and can solve their problems. The agency needs to do more to advertise this to citizens.

## 8. ACKNOWLEDGMENTS

Thanks to the Management of Rivers State Waste Management Agency (RIWAMA) and E-Sense Technologies Limited for the actualization of this project and for the contribution to this Paper.

## 9. REFERENCES

- [1] Agwu, M.O. (2012). 'Issues and Challenges of Solid Waste Management Practices in Port Harcourt City, Nigeria- a behavioural perspective'. *American Journal of Social and Management Sciences*. <https://pdfs.semanticscholar.org/9ee0/ded2c33732158db1c0cec92b67b947a92ea7.pdf>
- [2] Collins H.W (2014). 'Residential Development Dynamics in Port Harcourt Metropolis: Implication for Efficient Urban Planning'. *Journal of Environment and Earth Science*, 4(6). [www.iiste.org](http://www.iiste.org)
- [3] Elenwo, E.I. (2015). 'Solid Waste Management Practices in Port Harcourt Metropolis: Problems and Prospects'. *Journal of Geographic Thought and Environmental Studies*, 13(1). [http://www.academix.ng/documents/papers/1504110900\\_4652.pdf](http://www.academix.ng/documents/papers/1504110900_4652.pdf)
- [4] Ghosh S., Raju P., Saibaba J. and Varadan G. (2012). CyberGIS and Crowdsourcing – A new approach in E-Governance. <http://www.geospatialworld.net/paper/application/ArticleView.aspx?aid=24738>
- [5] Kallel A., Serbaji, M.M. and Zairi, M. (2016). 'Using GIS-Based Tools for the Optimization of Solid Waste Collection and Transport: Case Study of Sfax City, Tunisia'. *Journal of Engineering*, 2016 (2016). Available at: <http://dx.doi.org/10.1155/2016/4596849>
- [6] Kyessi, A. and Mwakalinga, V. (2009), 'GIS Application in Coordinating Solid Waste Collection: The Case of Sinza Neighbourhood in Kinondoni Municipality, Dar es Salaam City, Tanzania'. FIG Working Week 2009: Surveyors Key Role in Accelerated Development [https://www.fig.net/resources/proceedings/fig\\_proceedings/fig2009/papers/ts04b/ts04b\\_kvessi\\_mwakalinga\\_3219.pdf](https://www.fig.net/resources/proceedings/fig_proceedings/fig2009/papers/ts04b/ts04b_kvessi_mwakalinga_3219.pdf)
- [7] Neumann, A. (2007). *Encyclopedia of GIS*, Springer, 2007. pg 1262
- [8] Nigerian Communications Commission (2021). *Subscriber statistics*. <https://www.ncc.gov.ng/statistics-reports/subscriber-data>
- [9] Nna, N.J. and Pabon, B.G. (2012). 'Population, Environment and Security in Port-Harcourt', *IOSR Journal of Humanities and Social Science (JHSS)*, 2(1), PP 01-07. <http://www.iosrjournals.org/iosr-jhss/papers/Vol2-issue1/A0210107.pdf?id=5633>
- [10] Pickles, J. (1999). Arguments, debates and dialogues: the GIS-social theory debate and the concern for alternatives. In: P.A. Longley, M.F. Goodchild, D.J. Maguire, and D.W. Rhind, ed., *Geographical Information Systems: Principles, Techniques, Applications, and Management*. New York: Wiley, pp. 49-60.
- [11] Obuah, P.F and Okon, G.B. (2017). 'Environmental communication strategies of the Rivers State Waste Management Agency (RIWAMA): Implications for sustainable waste management in Nigeria'. *International Journal of Development and Sustainability*, 6(11), Pages 1541-1558. <https://isdsnet.com/ijds-v6n11-4.pdf>
- [12] Shoba, B. and Rasappan, K. (2013). 'Application of GIS in Solid Waste Management for Coimbatore City'. *International Journal of Scientific and Research Publications*, 3(10). <http://www.ijsrp.org/research-paper-1013/ijsrp-p2231.pdf>
- [13] Sibe, R.T. (2009), Challenges of Mapping Applications in Health and Academic Research in the Underdeveloped World – Case Study of The Niger Delta Region (Nigeria). [Online] Geospatial World. <https://www.geospatialworld.net/article/challenges-of-mapping-applications-in-health-and-academic-research-in-the-underdeveloped-world-case-study-of-the-niger-delta-region-nigeria/>
- [14] Sibe, R.T. (2010), Web-Based Application for the Rivers State Government in Nigeria: Spatial Component for the e-Service Portal. [Online] Geospatial World. <https://www.geospatialworld.net/article/web-based-gis-application-for-the-rivers-state-government-in-nigeria-spatial-component-of-the-e-service-portal/>
- [15] Sibe, R.T. (2014). Geospatial Technologies and Smart Governance: Prospects and Challenges for Africa. In: *Africa Geospatial Conference*. India: Geospatial Media and Communications
- [16] Tamunobereton-ari, I., mubo-Pepple, V. B. and Igbani, G. N (2012). 'Solid Waste Management Approach In Port Harcourt Municipality, Rivers State, Nigeria: The Effects On Public Health And The Environment'. *Asian Journal of Science and Technology*, 4(1), pp. 04 05.

<http://www.journalajst.com/sites/default/files/Download%201071.pdf>

- [17] Wizer, C.H. (2014). Residential Development Dynamics in Port Harcourt Metropolis: Implications for Efficient Urban Planning. *Journal of Environment and Earth Science*, 4(6).  
<http://www.iiste.org/Journals/index.php/JEES/article/view/11851>